The Astrophysical Journal, 978:158 (22pp), 2025 January 10 https://doi.org/10.3847/1538-4357/ad9584

Dwarf Galaxies with Radio-excess Active Galactic Nuclei in the Very Large Array Sky Survey

John-Michael Eberhard[1], Amy E. Reines[1], Hansung B. Gim[1], Jeremy Darling[2], and Jenny E. Greene[3]
[1] eXtreme Gravity Institute, Department of Physics, Montana State University, Bozeman, MT 59717, USA
[2] Center for Astrophysics and Space Astronomy, Department of Astrophysical and Planetary Sciences, University of Colorado, 389 UCB, Boulder, CO 80309-0389, USA
[3] Department of Astrophysical Sciences, Princeton University, Princeton, NJ 08544, USA
Received 2024 July 29; revised 2024 November 15; accepted 2024 November 19; published 2025 January 9

Abstract

We present a systematic search for radio active galactic nuclei (AGNs) in dwarf galaxies using recent observations taken by the Very Large Array Sky Survey (VLASS). To select these objects, we first establish a criterion to identify radio-excess AGNs using the infrared-radio correlation parameter, q, that describes the tight relation between radio and IR emission in star-forming galaxies. We find a 2σ threshold of $q < 1.94$ to select radio-excess AGNs, which is derived from a sample of ∼7000 galaxies across the full mass range in the NASA-Sloan Atlas that have radio and IR detections from VLASS and the Wide-Field Infrared Survey Explorer, respectively. We create catalogs of radio-excess AGNs and star-forming galaxies and make these available to the community. Applying our criterion to dwarf galaxies with stellar masses $M_\star \lesssim 3 \times 10^9\,M_\odot$ and redshifts $z \leqslant 0.15$, and carefully removing interlopers, we find 10 radio-excess AGNs with radio-optical positional offsets between ∼0″ and 2.″3 (0–2.7 kpc). Based on statistical arguments and emission line diagnostics, we expect the majority of these radio-excess AGNs to be associated with the dwarf host galaxies rather than background AGNs. Five of the objects have evidence for hosting AGNs at other wavelengths, and five objects are identified as AGNs in dwarf galaxies for the first time. We also identify eight variable radio sources in dwarf galaxies by comparing the VLASS epoch 1 and epoch 2 observations to Faint Images of the Radio Sky at Twenty-centimeters detections presented in A. E. Reines et al. (2020).

Unified Astronomy Thesaurus concepts: Dwarf galaxies (416); Intermediate-mass black holes (816); Radio sources (1358); Very Large Array (1766); Active galactic nuclei (16); AGN host galaxies (2017)

Materials only available in the online version of record: machine-readable tables

1. Introduction

The majority of black holes (BHs) belong to one of two populations: stellar mass BHs with masses $\sim 10\,M_\odot$ and supermassive black holes (SMBHs) with masses $\sim 10^{6-9}\,M_\odot$. BHs with masses between these extremes are often referred to as intermediate-mass black holes (IMBHs) and while hundreds of IMBHs with masses between $\sim 10^{5-6}\,M_\odot$ have been discovered in dwarf galaxies (e.g., A. E. Reines 2022), evidence for BHs with masses $\sim 10^{2-5}\,M_\odot$ is scarce (J. E. Greene et al. 2020 and references therein).

In addition to their rarity, IMBHs are objects of interest because they are critical to better understanding the origin of SMBHs. For SMBHs to reach their immense sizes, it is widely accepted that they evolved from smaller BHs, known as seeds, that grew through accretion and mergers. Different seeding models have been proposed (e.g., M. Volonteri et al. 2008; M. Volonteri & P. Natarajan 2009; B. Agarwal et al. 2012; A. Ricarte & P. Natarajan 2018; S. C. Rose et al. 2022), but it remains unclear as to which models are the most accurate, or if a combination of models is closest to reality. Each seeding model predicts a different size and quantity of seed BHs in the early Universe, and consequently, predicts a different distribution of modern-day IMBHs. Therefore, the discovery of more IMBHs may aid in constraining seeding models and improve our understanding of the way that SMBHs form and evolve.

We study dwarf galaxies to optimize the likelihood of discovering IMBHs since observational scaling relationships have shown that less massive galaxies host central BHs of lesser mass (e.g., J. Kormendy & L. C. Ho 2013; N. J. McConnell & C.-P. Ma 2013; A. E. Reines & M. Volonteri 2015; M. C. Bentz & E. Manne-Nicholas 2018; Z. Schutte et al. 2019). According to these relations, the masses of the BHs near the center of dwarf galaxies lie within the IMBH mass range.

Active galactic nuclei (AGNs) in dwarf galaxies can be studied over a variety of wavelengths, and each wavelength regime has proven to have a unique set of advantages and disadvantages. In the optical regime, AGNs have been identified using narrow emission line diagnostics (A. E. Reines et al. 2013; E. C. Moran et al. 2014; M. Molina et al. 2021; S. Salehirad et al. 2022) and by searching for broad Hα emission (e.g., J. E. Greene & L. C. Ho 2007; X.-B. Dong et al. 2012; A. E. Reines et al. 2013). The presence of broad Hα in conjunction with AGN-like narrow line ratios has been shown to be effective in discerning between AGNs and supernovae (SNe), which can also produce broad Hα lines in dwarf galaxies (V. F. Baldassare et al. 2016). One limitation of optical diagnostics is that they typically can only find BHs that are radiating at large fractions of their Eddington luminosity, which is fairly uncommon. Moreover, dust can extinguish optical light emitted from AGNs. X-ray emission is beneficial in detecting low-luminosity AGNs (e.g., S. M. Lemons et al. 2015; A. E. Reines & A. Comastri 2016; M. Mezcua et al. 2018;

L. J. Latimer et al. 2019), but X-ray observations require large exposure times, which is not practical for large-scale searches. Mid-IR observations also have the potential to identify AGNs, but when studying dwarf galaxies, it has proven difficult to separate the emission from intense star formation (SF) from the emission due to AGNs (K. N. Hainline et al. 2016; S. Satyapal et al. 2018; L. J. Latimer et al. 2021).

Radio searches for AGNs have some advantages compared to other wavelength regimes. AGNs almost always create radio emission at centimeter wavelengths (L. C. Ho 2008 and references therein). Strong radio signals are primarily produced by synchrotron emission in the form of radio jets. Weaker radio signals from AGNs can come from a variety of sources, including AGN-driven winds, thermal free–free emission from photoionized gas, and coronal activity from the accretion disk (see F. Panessa et al. 2019 and references therein). Another advantage of using radio searches is that radio emission is nearly unaffected by interstellar dust extinction. These factors, combined with the substantial area covered by existing radio surveys, make the use of radio observations an excellent method for conducting large-scale searches for AGNs. For these reasons, previous radio searches have been used to identify AGNs in dwarf galaxies, using data collected by the Very Large Array (M. Mezcua et al. 2019; A. E. Reines et al. 2020).

One difficulty with working in the radio regime, however, is that radio emission is not unique to AGNs. SF creates radio emission that can mimic or mask the radio signals created by AGNs (e.g., A. E. Kimball et al. 2011; J. J. Condon et al. 2013; N. L. Zakamska et al. 2016). SF creates H II regions, which in turn produce thermal emission via free–free emission (e.g., J. Caplan & L. Deharveng 1986), while supernova remnants (SNRs) and SNe create nonthermal radio emission via synchrotron radiation, as cosmic-ray electrons from SNRs and SNe are accelerated in galactic magnetic fields (see the J. J. Condon 1992 review).

In this work, we identify galaxies with AGNs by finding sources with radio fluxes from the VLA Sky Survey (VLASS) that lie significantly above the well-known IR-radio relation for star-forming galaxies (SFGs). We derive a criterion for discerning between SF and AGNs, using galaxies of all masses in the NASA-Sloan Atlas (NSA) with detections in VLASS and Wide-Field Infrared Survey Explorer (WISE), and then apply our method to dwarf galaxies specifically. This paper is organized as follows: In Section 2, we describe the data and catalogs we use in this work. In Section 3, we explain how we match all the galaxies from the NSA to VLASS radio sources and develop a cutoff between emission from SF and emission from radio-excess AGNs. We analyze the properties of all the radio-excess AGN hosts and compare them to results from the literature in Section 4. In Section 5, we apply the cutoff found in Section 3 to lower mass galaxies to find dwarf galaxies with radio-excess AGNs. We analyze their properties and compare them to the full sample of radio-excess AGNs. We conclude with a summary and a discussion of our discoveries in Section 6. For consistency with A. E. Reines et al. 2020, we use $H_0 = 73\ \mathrm{km\ s^{-1}\ Mpc^{-1}}$ throughout.

2. Data

In this paper, we match the radio sources detected by VLASS to galaxies in the NSA, similar to how A. E. Reines et al. (2020) matched radio sources from the Faint Images of the Radio Sky at Twenty-centimeters (FIRST) Survey to the NSA. However, several key differences between the data used here and A. E. Reines et al. (2020) make this study worthwhile and novel.

One major difference is the quality of VLASS compared to FIRST. FIRST had an angular resolution of 5″ and a median rms sensitivity of $\sim$100 μJy beam^{-1}, and covered 10,000 deg^2 of sky (R. L. White et al. 1997). VLASS, in contrast, has an angular resolution of 2.″5 and covers 33,885 deg^2 of sky (all of the sky above $-40°$ decl.). The rms sensitivity per epoch of VLASS is comparable to FIRST (120 μJy beam^{-1}), but the expected 1σ sensitivity is 70 μJy beam^{-1} once its three planned epochs are complete (M. Lacy et al. 2020). Furthermore, FIRST concluded its observations in 2011 and VLASS is currently still observing. The difference in time between observations also results in finding transient sources that were not bright enough for detection a decade ago.

Due to its higher angular resolution, VLASS can separate single sources in FIRST into multiple sources and find radio lobes as radio sources that do not coincide with their host galaxies. We minimize the likelihood of matching radio sources to unrelated galaxies by utilizing a small crossmatching radius between surveys (see Section 3.1).

Another critical difference between this paper and A. E. Reines et al. (2020) is the use of an updated NSA catalog. A. E. Reines et al. 2020 utilized v0_1_2 of the NSA, which extended to a redshift of $z = 0.055$, whereas the version used in this paper (v1_0_1) extends to a redshift of $z = 0.15$. Between the more recent and higher quality radio data from VLASS and the larger sample of galaxies from the newer version of the NSA, we find new candidates for radio-excess AGNs within dwarf galaxies than those found by A. E. Reines et al. (2020).

2.1. Very Large Array Sky Survey

The Very Large Array Sky Survey (VLASS) is performed by the National Science Foundation's (NSF's) Karl G. Jansky Very Large Array (VLA) in the B configuration in the S band (2–4 GHz). Observations began in 2017 September and the survey is expected to complete three epochs by the end of 2024. As of the time of this paper's submission, two of the three planned epochs are complete and data products have been provided as part of the Canadian Initiative for Radio Astronomy Data Analysis (CIRADA) program,[4] which partnered with the National Radio Astronomy Observatory (NRAO)[5] and the Canadian Astronomy Data Centre.

We retrieve the entire epoch 2 catalog from the CIRADA webpage and process the data to remove duplicate radio sources and images with poor quality flags. Based on the beam size and positional uncertainty of VLASS images, the CIRADA catalog flags duplicates as sources within 2″ of another source. When duplicates are found, preference is given to the source with the highest ratio peak flux density to local rms. Restricting by the duplicate flag in the CIRADA catalog restricts the catalog to only include sources that are unique or preferred components. By restricting with the quality flag, we remove every radio source whose peak brightness is less than

[4] CIRADA is funded by a grant from the Canada Foundation for Innovation 2017 Innovation Fund (Project 35999), as well as by the Provinces of Ontario, British Columbia, Alberta, Manitoba, and Quebec.

[5] The NRAO is a facility of the NSF operated under cooperative agreement by Associated Universities, Inc.

five times larger than the local rms of its respective image. Of the 2,995,271 sources in the original catalog, 1,125,370 (38%) of the sources are removed due to their low quality flags and a further 174,749 (6%) of the sources are removed based on their duplicate flags. This leaves 1,695,152 radio sources in our sample with signal-to-noise ratio (S/N) cuts at the 5σ level.

2.2. NSA

The NSA v1_0_1 is a catalog of images and parameters for local galaxies, with redshift $z \leqslant 0.15$, including data taken from surveys in the near-IR, optical, and UV regimes. The emphasis of the catalog is on the inclusion of parameters derived from the Sloan Digital Sky Survey (SDSS) and the Galaxy Evolution Explorer (GALEX; D. G. York et al. 2000; M. R. Blanton et al. 2005). The version of the NSA catalog we use is based on the observations in SDSS DR11, with a sky coverage area of 14,555 deg^2.

Photometric measurements in the NSA are derived by making image mosaics and rephotometering the images from the *ugriz* bands in SDSS and the far-UV and near-UV bands from GALEX. The version used in this work utilizes elliptical Petrosian apertures to report the K-corrected absolute AB magnitudes in each of the bands. K-corrections are determined using the `kcorrect` package (M. R. Blanton & S. Roweis 2007), which fits SDSS and broadband GALEX fluxes using templates based on the stellar population synthesis models of G. Bruzual & S. Charlot (2003) and the nebular emission line models of L. J. Kewley et al. (2001). The stellar mass estimates that correspond to the best fits are included in the NSA.

The majority of redshifts in the NSA are derived from SDSS spectra, but in some cases, redshifts are taken from other sources, including the NASA/IPAC Extragalactic Database (NED), the Six-degree Field Galaxy Redshift Survey, the Two-degree Field Galaxy Redshift Survey, the CfA Redshift Survey, and Arecibo Legacy Fast Arecibo L-Band Feed Array.

2.3. WISE

WISE is a NASA IR space telescope that performed an all-sky astronomical survey starting January 2010. WISE used a 40 cm diameter telescope in four IR bands: W1, W2, W3, and W4, which are centered at wavelengths of 3.4, 4.6, 12, and 22 μm, with angular resolutions of $6\farcs1$, $6\farcs4$, $6\farcs5$, and $12\farcs0$, respectively (E. L. Wright et al. 2010). Observations and S/N for each of the IR bands are recorded in the AllWISE source catalog[6] (E. L. Wright et al. 2019), and are only included in the catalog if at least one of the four bands has $S/N > 5$. We utilize the "profile-fitting" photometric magnitudes from the AllWISE catalogs, which are optimized for unresolved sources.

3. Finding Radio-excess AGNs in VLASS

To distinguish between radio emission dominated by SF and emission dominated by AGNs, we compare the radio luminosities from VLASS to IR luminosities from WISE. We utilize the infrared-radio correlation (IRRC) parameter q, as has been done in previous papers (e.g., M. S. Yun et al. 2001; J. J. Condon et al. 2002; A. Del Moro et al. 2013; J. Delhaize et al. 2017; I. Delvecchio et al. 2021) to find galaxies with radio emission significantly higher than expected from SF. We study the full sample of galaxies from the NSA in this section to better quantify the scatter and develop an accurate method for discerning between SF-related emission and emission from AGNs.

3.1. NSA-VLASS-WISE Sample

We retrieve the full catalog of galaxies in the NSA to create a parent sample of 641,409 galaxies. We crossmatch the NSA and VLASS coordinates with a crossmatching radius of $2\farcs5$, resulting in finding 13,688 galaxies within the NSA with associated VLASS detections.

We then crossmatch our sample of NSA galaxies with VLASS detections to the AllWISE catalog, again employing a crossmatching radius of $2\farcs5$ and selecting the closest IR source if multiple sources are found within the radius. We require the WISE detections to be high-quality measurements with $S/N \geqslant 5$ in the W4 band. This ensures an accurate distribution of IRRC values for the galaxies in our sample and enables us to determine a reliable cutoff for identifying radio-excess AGNs (see Section 3.3). We note that while we do not use the galaxies with $S/N < 5$ to calculate the IRRC cutoff, we do include them in our AGN catalog provided in the Appendix.

For the purposes of determining the IRRC distribution, we also remove sources that have underestimated fluxes in WISE. The "profile-fitting" magnitudes we use from the WISE catalog are optimized for pointlike sources, meaning that the fluxes of resolved sources are systematically underestimated. We therefore remove all extended sources from our sample, where we consider extended sources to be any sources with a W4 profile-fit photometry goodness of fit (χ^2) above 3 (the same criterion used by the AllWISE catalog to flag extended sources). By applying this criterion, we remove 219 extended IR sources from our sample.

Once these sources are removed, we are left with a total of 6,772 galaxies with reliable W4 measurements. These galaxies have high values of S/N in all of the WISE bands. All have W2 and W3 detections with $S/N > 5$. Only six galaxies have W1 magnitudes with $S/N < 5$, and even these have $S/N \geqslant 4$. Restricting by W4 therefore results in finding galaxies that have strong detections in all bands of WISE. We refer to the sample of galaxies in the NSA with VLASS and strong WISE detections as the NSA-VLASS-WISE sample.

3.2. Removal of Mid-IR AGNs

To find radio-excess AGNs within our sample, we will need to differentiate between the emission from SF and the emission from radio-excess AGNs. This will be done by comparing the ratio of IR and radio luminosities (see Section 3.3) under the assumption that the IR emission comes primarily from SF. To be able to make this assumption, we remove galaxies whose mid-IR emission is characteristic of AGNs. We compare the WISE IR colors (W1–W2 and W2–W3) for the galaxies in the NSA-VLASS-WISE sample in a color–color diagram (see Figure 1). We exclude mid-IR AGNs by removing galaxies that lie within the T. H. Jarrett et al. (2011) AGN selection box or above the D. Stern et al. (2012) AGN cutoff, finding 1103 that fit these criteria.

Given the high S/N for the W4 observations in our sample, we consider using the WISE four-band AGN selection criteria

[6] This publication makes use of data products from WISE, which is a joint project of the University of California, Los Angeles, and the Jet Propulsion Laboratory/California Institute of Technology, funded by the National Aeronautics and Space Administration.

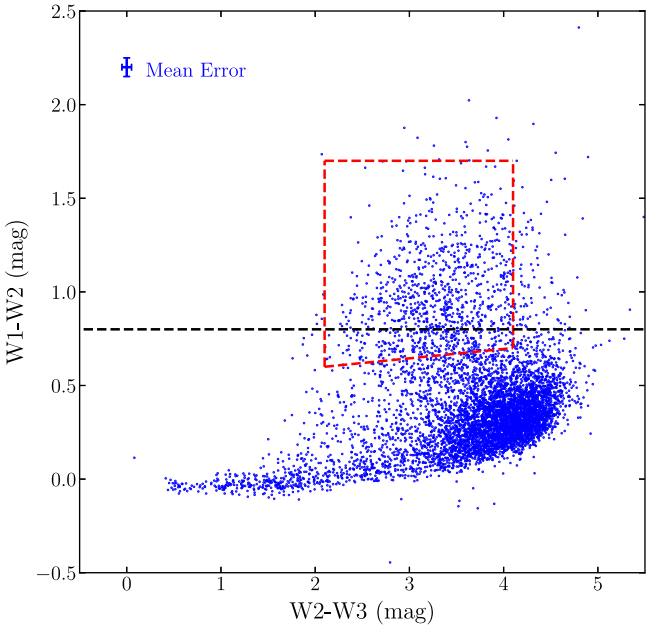

Figure 1. WISE color–color diagram for all galaxies in the NSA-VLASS-WISE sample. The T. H. Jarrett et al. (2011) AGN selection box is shown in red and the D. Stern et al. (2012) AGN cutoff line is shown in black. We remove all galaxies found within the selection box or the cutoff line to limit the effect of mid-IR AGN emission on the IR luminosities used in the IRRC (Section 3.3). The mean error bars for the data are shown in the upper left corner.

from S. Mateos et al. (2012) instead of the criteria from T. H. Jarrett et al. (2011) and D. Stern et al. (2012). However, the four-band method only identifies 620 objects mid-IR AGNs, compared to the 1103 mid-IR AGNs found above. To minimize the likelihood of including mid-IR AGNs in our sample, we opt to use the combined T. H. Jarrett et al. (2011) and D. Stern et al. (2012) criteria, as this identifies a larger number of AGNs.

We note that the percentage of our sample (Section 3.1) identified as mid-IR AGNs (16%) is larger than is expected for the general galaxy population. This is likely due to our restriction on the W4 S/N, which means our sample preferentially contains galaxies with higher overall IR luminosities. Galaxies with higher IR luminosities in turn are more likely to host IR-selected AGNs, as evidenced by the sample studied in A. D. Goulding & D. M. Alexander (2009), which found 27% of IR-bright galaxies to have AGNs.

We also note that the T. H. Jarrett et al. (2011) and D. Stern et al. (2012) cutoffs were not established for radio-selected galaxies. So, while the cutoffs we use identify the majority of mid-IR AGNs in our sample, they may not properly account for the full scatter (both real and due to a low S/N) of our radio-selected sample, and fail to find all of the mid-IR AGNs (e.g., A. E. Truebenbach & J. Darling 2017). Nevertheless, we work with the 5,669 remaining galaxies under the assumption that the IR emission for the galaxies is dominated by SF.

3.3. The IRRC

We develop a method for distinguishing between radio emission from SF and AGNs by analyzing the IRRC parameter for our sample. The IRRC parameter q describes the tight relation between radio and IR emission in SFGs and takes the following form:

$$q = \log\left[\frac{L_{\rm IR}}{3.75 \times 10^{12}\, L_{1.4\,\rm GHz}}\right] \quad (1)$$

where $L_{\rm IR}$ is in units of watts and $L_{1.4\,\rm GHz}$ is in units of watts per hertz (e.g., T. de Jong et al. 1985; G. Helou et al. 1985). $L_{\rm IR}$ is frequently reported in terms of far-IR (FIR) wavelengths (40–120 μm) or total-IR (TIR) wavelengths (8–1000 μm). For SFGs in the local universe, M. S. Yun et al. (2001) found that $q_{\rm FIR} = 2.34 \pm 0.26$ dex for FIR wavelengths, and E. F. Bell (2003) found that $q_{\rm TIR} = 2.64 \pm 0.26$ dex for TIR wavelengths.

The IRRC parameter has also been used to find radio-excess AGNs by looking for sources that have excessively low values of q, indicating high amounts of radio emission that cannot be described by SF. However, the level of radio emission that is considered to be significantly high varies between studies. J. J. Condon et al. (2002) defined radio-excess AGNs as objects with radio emission three times larger than expected from the IRRC, while M. S. Yun et al. (2001) defined radio-excess AGNs as objects with radio luminosities that are five times greater than the value predicted by the IRRC or larger. The cutoff in M. S. Yun et al. (2001) came from finding sources with q values that were lower than three times the rms scatter below the mean value of q for the SFGs. M. Bonzini et al. (2013) found an AGN cutoff using the full distribution of q in their sample, defining radio-excess AGNs as objects with q values that were lower than two standard deviations (σ_q) below the mean value (μ_q). A. Del Moro et al. (2013) and J. Delhaize et al. (2017) performed a similar analysis, but used a cutoff of $3\sigma_q$ below μ_q.

I. Delvecchio et al. (2021) elaborated on the reason that such a variety of methods exist, explaining that defining the cutoff between AGN and SF radio emission is a difficult and somewhat arbitrary task. Changing the cutoff to a lower q increases the purity of finding AGNs, but at the cost of finding all of the AGNs. I. Delvecchio et al. (2021) determined an ideal cutoff for q by testing various thresholds and identifying the cutoffs that resulted in the best compromise between reaching low levels of cross-contamination between the AGN and SF populations and finding a large number of SFGs beneath the threshold. They found the cutoff at $q = q_{\rm peak} - 2\sigma$ to give the best trade-off between completeness and cross-contamination, where $q_{\rm peak}$ and σ are the peak value and standard deviation of the q distribution for the population, respectively. We similarly adopt the $q = q_{\rm peak} - 2\sigma$ criteria in this work to find the maximum number of AGNs with minimal contamination from the SF population.

To calculate the distribution of q values for our sample (using Equation (1)), we convert the 3 GHz flux densities from VLASS to 1.4 GHz luminosities. Just as M. Novak et al. (2017) converted from VLA-COSMOS 3 GHz data to 1.4 data, we convert the 3 GHz flux densities from VLASS to 1.4 GHz luminosities with the following equation:

$$L_{\nu_1} = \frac{4\pi D_L^2}{(1+z)^{1+\alpha}}\left(\frac{\nu_1}{\nu_2}\right)^{\alpha} S_{\nu_2}. \quad (2)$$

Here, L_{ν_1} is the rest-frame radio luminosity at the rest-frame frequency ν_1, derived from the observed flux S_{ν_2} at the observed-frame frequency ν_2, redshift z, luminosity distance D_L, and spectral index α. To convert VLASS observations to radio luminosities that can be used in Equation (1), we set

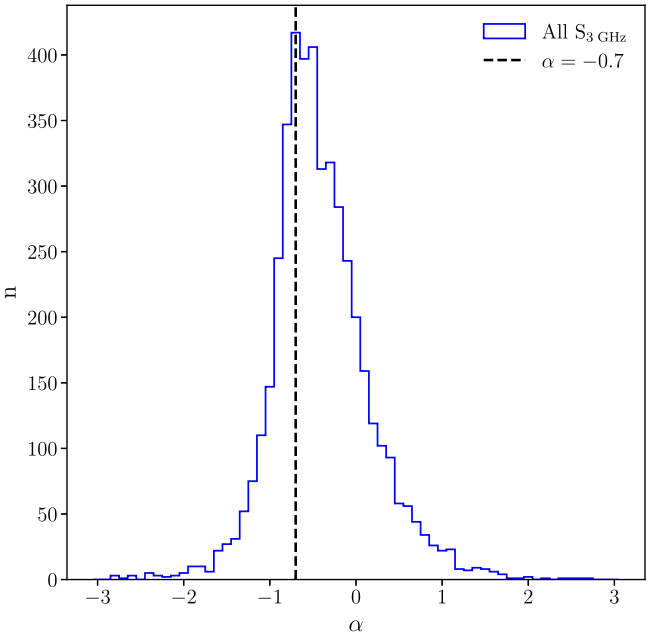

Figure 2. Distribution of spectral indices for the galaxies in the NSA-VLASS-WISE sample with corresponding FIRST observations. The distribution peaks at a similar value to the standard value of $\alpha = -0.7$, which is commonly assumed to be the median value for SFGs.

$\nu_1 = 1.4$ GHz and $\nu_2 = 3$ GHz. As was done in M. Novak et al. (2017), we assume that each radio source in our sample has a radio spectrum that can be described as a simple power law ($S_\nu \propto \nu^\alpha$) where S_ν is the monochromatic flux at frequency ν and α is the spectral index, resulting in the K-correction of $K(z) = (1+z)^{-(1+\alpha)}$ seen in Equation (2).

For ∼75% of the sources, we find α directly by matching the VLASS catalog to the FIRST catalog, with a crossmatching radius of 5″ (the resolution of FIRST). The distribution of α for galaxies in the NSA-VLASS-WISE sample with FIRST detections is shown in Figure 2. The values of the spectral indices are largely found between −2 and 2 and the distribution peaks at $\alpha \sim -0.7$. This peak value matches well with the standard $\alpha = -0.7$ that is commonly assumed in the literature (e.g., J. J. Condon et al. 2012; M. Novak et al. 2017; V. Smolčić et al. 2017). As such, for the sources without FIRST detections, we assume a spectral index of $\alpha = -0.7$ in Equation (2).

We estimate $L_{\rm TIR}$ using data from the W4 band of WISE, centered at a wavelength of 22 μm. C.-N. Hao et al. (2011) reported that $L_{\rm TIR} \approx 8.33\, L_{25\mu{\rm m}}$ and T. H. Jarrett et al. (2013) showed that the flux densities at 22 μm and 25 μm are approximately equal. These relations were established using samples of nearby galaxies that covered a wide range of color, luminosity, and stellar mass (including dwarf galaxies). Therefore, we deem it appropriate to use these relations on our full sample to convert directly from W4 luminosities to TIR luminosities.

Using the assumptions above, we calculate q for all of the galaxies in the NSA-VLASS-WISE sample that are not classified as mid-IR AGNs and find the distribution shown in Figure 3. We fit a Gaussian to the distribution and find that the sample peaks at $q_{\rm peak} = 2.62$, matching well with the results from E. F. Bell (2003). We find the scatter of the distribution to be $\sigma = 0.34$, resulting in the 2σ cutoff of $q < 1.94$. When we apply this cutoff to our NSA-VLASS-WISE sample (excluding mid-IR AGNs), we find 625 (11%) of the galaxies to host radio-excess AGNs. The percentage of radio AGNs found in our sample is larger than expected for the general galaxy population. This increase can be attributed to our selection of galaxies with VLASS detections with high S/N (see Section 2.1). When we require the galaxies in our sample to have high-quality radio data, we preferentially find objects that are louder in the radio regime, which results in finding a larger percentage of AGNs. I. Delvecchio et al. (2021) experienced a similar phenomenon: when they restricted their galaxy sample to only include sources with strong detections in the radio regime, they found that ∼16% of the population with high S/N radio observations were identified as radio AGNs.

We also consider how the distribution of q values may change with the inclusion of galaxies with W4 S/N < 5. When we examine the distribution of the galaxies with a W4 S/N < 5, we find that it has much lower values of q compared to the distribution of galaxies with high W4 S/N data (see Figure 4). In fact, 93% of the galaxies with a W4 S/N < 5 have $q < 1.94$ (our criterion established above) and are likely radio-excess AGNs. Moreover, this statistic does not consider the fact that the q values calculated with W4 S/N < 5 are upper limits, meaning that the true percentage of galaxies with $q < 1.94$ could be even higher. As such, the low S/N observations largely do not affect the distribution of the SFGs. Since the radio-excess AGN cutoff was established using a population dominated by SFGs, the effect that the W4 S/N < 5 galaxies have on the radio-excess AGN cutoff is minimal.

4. Properties of the NSA-VLASS-WISE Sample

4.1. Radio Source Properties

We consider the characteristics of all the radio sources in the NSA-VLASS-WISE sample that are not mid-IR-selected AGNs and compare the properties of the galaxies selected as radio-excess AGN hosts to the remaining galaxies. For simplicity of nomenclature, we refer to all galaxies not identified as radio-excess AGN hosts as being SF consistent, even though they could still contain AGNs, albeit AGNs that do not have radio emission greater than the emission predicted to come from SF.

We examine the radio sources of the two populations to see if they are pointlike by analyzing the distribution of the full width at half-maximum (FWHM) of the deconvolved major axis ($\Psi_{\rm maj}$) of the sources. VLASS can probe down to a size of ∼0.″3 and below this angular size, $\Psi_{\rm maj}$ values are unresolved and are recorded in the VLASS catalog as having a value of 0″ (Y. A. Gordon et al. 2021). We create normalized histograms of $\Psi_{\rm maj}$ values for the radio-excess AGNs and the SF-consistent population (see Figure 5). We find that the fraction of sources with $\Psi_{\rm maj} = 0''$ is larger for the radio-excess AGN population (16%) than the SF-consistent population (11%). Additionally, the AGN population contains a larger percentage of compact sources, with a median value of $\Psi_{\rm maj} = 1.''2$ while the SF-consistent population has a median value of $\Psi_{\rm maj} = 2.''4$ (both medians are calculated by ignoring the 0″ values). A two-sample Kolmogorov–Smirnov (K-S) test returns a p-value of $p < 0.001$, indicating that the distributions of $\Psi_{\rm maj}$ originate from different parent samples.

For decades, radio galaxies have been divided into two major types: Fanaroff–Riley Class I (FR I) and Fanaroff–Riley Class II (FR II; B. L. Fanaroff & J. M. Riley 1974). FR I sources are

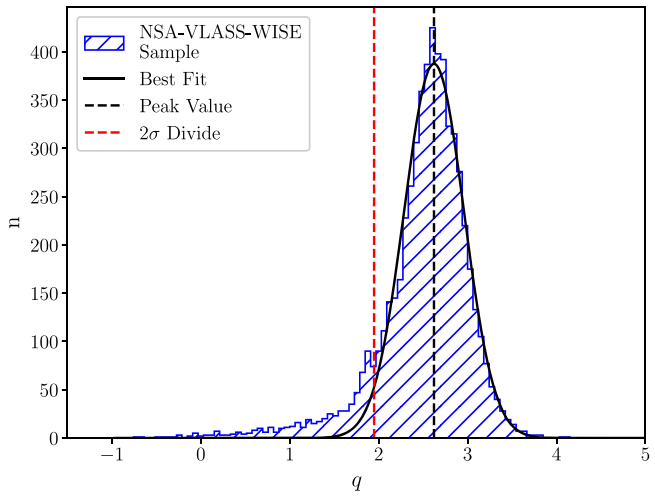

Figure 3. Distribution of q for the galaxies in the NSA-VLASS-WISE sample that are not classified as mid-IR AGNs (see Figure 1). When a Gaussian is fit to the distribution, it peaks at $q_{\rm peak} = 2.62$ and has a scatter of $\sigma = 0.34$, resulting in a 2σ threshold of $q < 1.94$ for identifying radio-excess AGNs.

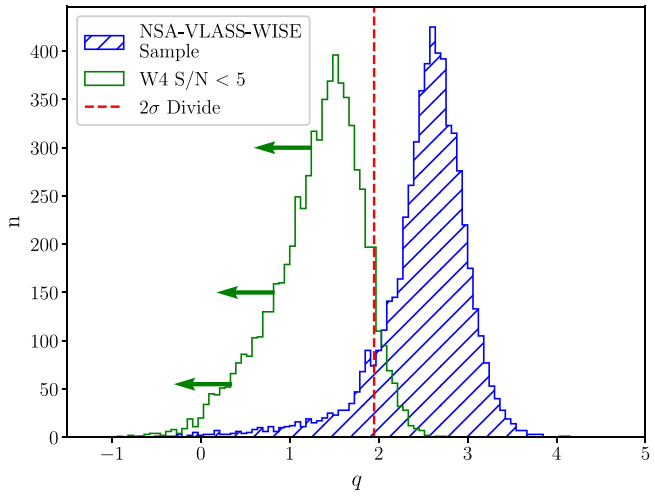

Figure 4. Distribution of q for the galaxies in the NSA-VLASS-WISE sample (blue) and for galaxies with WISE W4 observations with S/N < 5 (green). The q values calculated for the galaxies with W4 S/N < 5 are upper limits, as indicated by the arrows. The 2σ radio-excess cutoff derived from Figure 3 is shown as a red dashed line. The vast majority of the galaxies with W4 S/N < 5 have q values inconsistent with SFGs and are dominated by a population of radio-excess AGNs.

core dominated and have radio emission that peaks near the center of their host galaxies and fades with distance. FR II sources are dominated by their jets and lobes and brighten near the edge of their hosts. Given the relatively small angular size of the radio sources in the radio-excess AGN population, we hypothesize that our sample of radio-excess AGNs primarily consists of core-dominated sources. This result is expected since in the local universe, the majority of radio galaxies are FR I sources (M. J. Ledlow & F. N. Owen 1995; F. Govoni et al. 2000; P. N. Best et al. 2005). Furthermore, in crossmatching the VLASS and NSA catalogs, we required the radio sources to be located close to the center of their host galaxies, constraining our sample to preferentially detect FR I sources.

We also compare the 3 GHz radio luminosities of the two populations (see Figure 5). The distribution of radio luminosities for the SF-consistent population has a median of $\log(L_{3\ \rm GHz}/{\rm W\ Hz^{-1}}) = 22.1$ and an FWHM of 1.3 and the radio-excess AGN population has a median radio luminosity of $\log(L_{3\ \rm GHz}/{\rm W\ Hz^{-1}}) = 22.6$ with a FWHM of 1.9. A two-sample K-S test of the distributions reveals that the probability that the two distributions come from the same original distribution is extremely low, with a probability of $p < 0.001$. We note that the two populations have significant overlap in radio luminosities despite being statistically different. This overlap reiterates the fact that radio luminosity alone is often not enough to determine if a source is a radio-excess AGN. Using the definition of radio-quiet AGNs from L. Miller et al. (1990) as AGNs with radio luminosities $L_\nu < 10^{24}$ W Hz^{-1}, we see that both the SF-consistent population and the radio-excess AGN population can host radio-quiet AGNs. Despite the overlap between the two samples, the radio-excess AGN radio luminosity distribution has a prominent tail toward high luminosity, which results in the small p-value of the two-sample K-S test. The SF-consistent population has a maximum radio luminosity of $\log(L_{3\ \rm GHz}/{\rm W\ Hz^{-1}}) = 23.9$, while the radio-excess AGN population has a maximum of $\log(L_{3\ \rm GHz}/{\rm W\ Hz^{-1}}) = 26.0$. As such, it could be hypothesized that a 3 GHz luminosity above $\sim 10^{24}$ W Hz^{-1} is indicative of a radio-loud AGN.

4.2. Host Galaxies

We compare the populations of galaxies by investigating their stellar masses and $g - r$ colors taken from the NSA. Normalized histograms of the estimated stellar masses (M_*) of the two populations are shown in Figure 5. The mass distribution of an SF-consistent population has a median stellar mass of $\log(M_*/M_\odot) = 10.6$ with an FWHM of 0.82 and the radio-excess AGN distribution has a median of $\log(M_*/M_\odot) = 10.9$ and an FHWM of 0.92. The two-sample K-S test returns a p-value of $p < 0.001$, indicating that the two distributions originate from totally different parent samples.

The $g - r$ colors of the two populations, calculated from the absolute AB magnitudes in the NSA, are also shown in Figure 5. The SF-consistent population has a median color of $g - r = 0.65$ with an FWHM of 0.40 and the radio-excess AGN population has a median of 0.75, with an FWHM of 0.25. The two-sample K-S test returns a p-value of $p < 0.001$, showing that the two distributions are distinct and are unlikely to have come from the same parent distribution. Overall, the population of radio-excess AGN hosts appears to be redder and more massive than the SF-consistent galaxies.

We also determine that the SF-consistent galaxies tend to be late-type galaxies. We quantify this in Figure 6 by comparing the (inverse) concentration indices of the two populations, calculated using the half-light and 90%-light Petrosian radii from the NSA. The (inverse) concentration index comes from K. Shimasaku et al. (2001) and is defined as $C = r_{50}/r_{90}$, where r_{50} and r_{90} are the half-light and 90%-light radii, respectively. The divide between early and late-type galaxies, as established by K. Shimasaku et al. (2001), is also shown, with the peak of the radio-excess AGN population being found on the early-type side of the divide and the peak of the SF-consistent population being found on the late-type side. In addition to being visually distinct, the distributions are statistically different, with the two-sample K-S test returning a p-value under 0.001. The (inverse) concentration indices also show that the radio-excess AGN hosts are more centrally concentrated than the SF-consistent galaxies. The compactness of the AGN hosts could

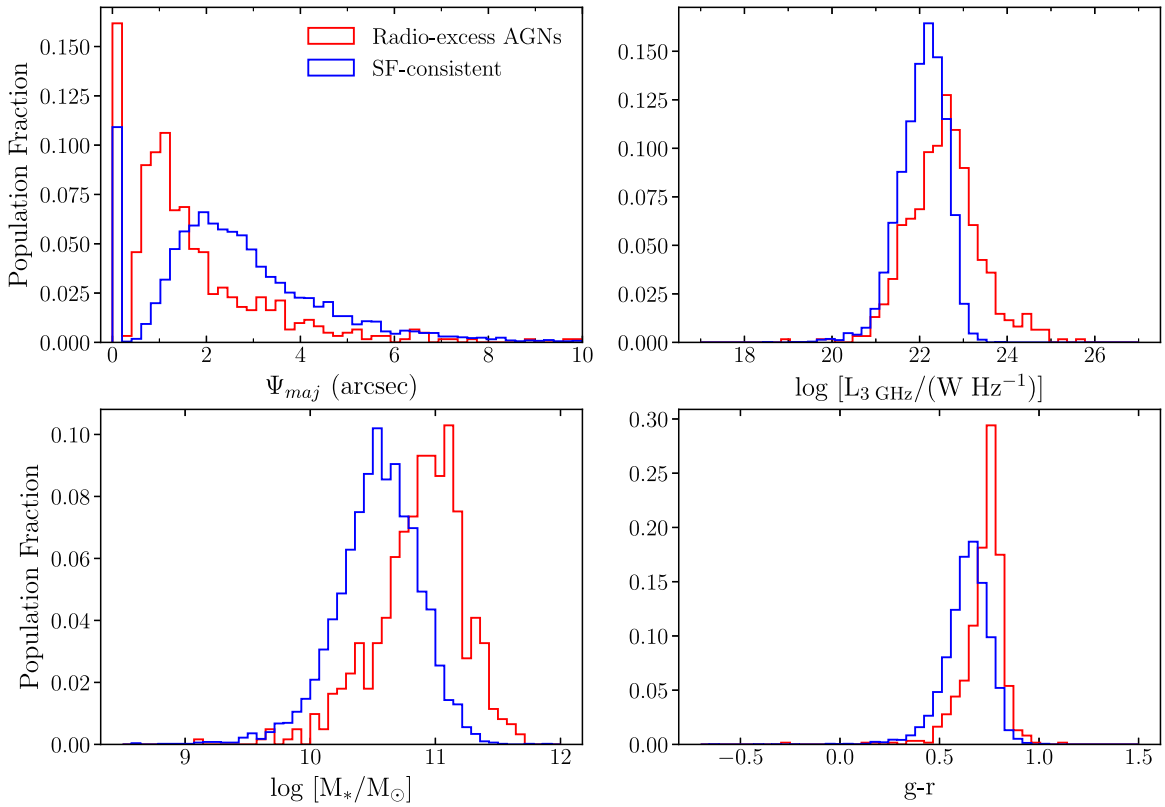

Figure 5. Histograms comparing the radio-excess AGN host population (red) to the SF-consistent population (blue) of the galaxies in the NSA-VLASS-WISE sample that are not mid-IR AGNs. Top left: deconvolved major axis sizes, Ψ_{maj}. Values closer to zero are indicative of more compact sources. Top right: integrated 3 GHz radio luminosities of the radio sources. Bottom left: stellar masses of the host galaxies. Bottom right: $g - r$ colors of the host galaxies. In general, the radio-excess AGNs have radio sources that are more compact and host galaxies that are more massive and redder than the SF-consistent galaxies.

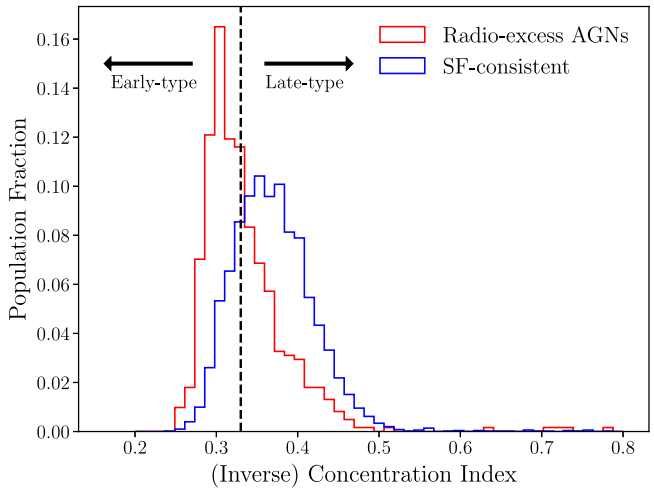

Figure 6. Histogram of the (inverse) concentration indices, defined as r_{50}/r_{90}, for the radio-excess AGN and SF-consistent populations in the NSA-VLASS-WISE sample. K. Shimasaku et al. (2001) divide between late- and early-type galaxies is shown as a dashed line. Notably, the radio-excess AGN population peaks in the early-type regime, while the SF-consistent population peaks in the late-type regime.

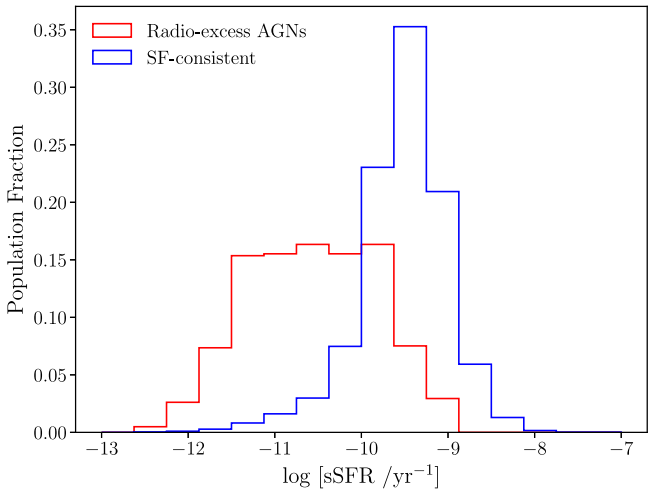

Figure 7. sSFRs for the radio-excess AGN and SF-consistent populations in the NSA-VLASS-WISE sample. The SF-consistent population predictably has higher sSFRs, while the radio-excess AGNs have a wider spread and a larger fraction of its population with lower values of sSFR. The low values of sSFR in the AGN population could be caused by SF quenching from the AGNs.

be driven by the presence of the AGN as a central point source, although given that the radio properties of an AGN rarely correlate well with their optical properties (e.g., P. N. Best et al. 2005), we find this to be unlikely. It is more likely that AGNs reside in more centrally concentrated galaxies than the presence of a radio AGN influences the calculation of the (inverse) concentration indices.

We also consider the specific star formation rate (sSFR) of the galaxies to see if there is evidence of quenching of SF within the AGN hosts (see Figure 7).

We calculate star formation rates (SFRs) using IR data from WISE and the following SFR_{IR} equation from

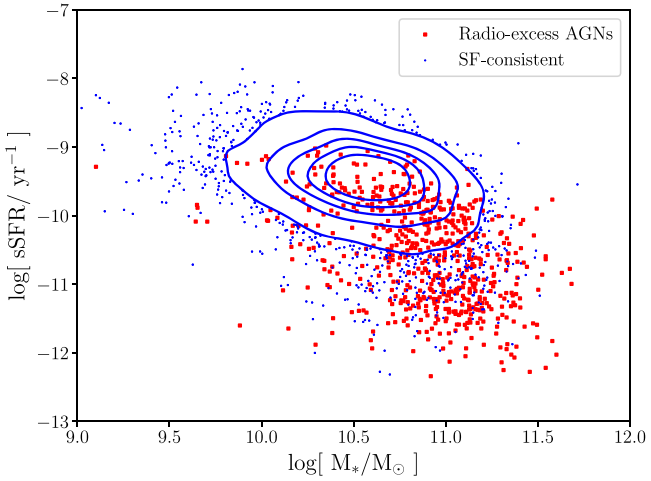

Figure 8. sSFRs vs. stellar masses for the radio-excess AGN hosts and SF-consistent populations in the NSA-VLASS-WISE sample. The blue contours and points show the distribution of the SF-consistent galaxies, and the filled red squares show the radio-excess AGN hosts. At stellar masses above $\sim 10^{10.7}\,M_\odot$, the radio-excess AGN hosts have consistently lower sSFRs than the SF-consistent galaxies. Below this mass, however, the sSFRs of the radio-excess AGN hosts often have similar values to the sSFRs of the SF-consistent galaxies.

E. J. Murphy et al. (2011):

$$\frac{\mathrm{SFR_{IR}}}{M_\odot\ \mathrm{yr^{-1}}} = 3.88 \times 10^{-44}\left(\frac{L_{\mathrm{TIR}}}{\mathrm{erg\ s^{-1}}}\right) \quad (3)$$

where L_{TIR} is the TIR luminosity. This equation was derived by integrating the output spectrum from Starburst99 stellar population models (C. Leitherer et al. 1999) over the wavelength range $912\,\text{Å} < \lambda < 3646\,\text{Å}$. The models used a Kroupa (P. Kroupa 2001) initial mass function, with a slope of -1.3 for masses between 0.1 and $0.5\,M_\odot$ and -2.3 for masses between 0.5 and $100\,M_\odot$. We use the L_{TIR} values found in Section 3.3 to calculate the SFRs. We divide the SFRs by the stellar masses from the NSA to find the sSFRs.

The SF-consistent population has a sharper peak at higher sSFRs than the AGN population, with a median value of $\log(\mathrm{sSFR/yr^{-1}}) = -9.5$ and an FWHM of 1.2 compared to the AGN population's median of $\log(\mathrm{sSFR/yr^{-1}}) = -10.6$ and FWHM of 1.7. The sSFR distributions are also statistically different and the two-sample K-S test returns a p-value below 0.001.

Overall, the sSFR distributions show that the AGN population has a larger percentage of galaxies with lower amounts of SF per unit mass, which could be indicative of the AGN quenching SF in their host galaxies. However, when we compare sSFRs to stellar masses (Figure 8), we find that this is largely true only for larger mass galaxies. Radio-excess AGN host galaxies with stellar masses below $\sim 10^{10.7}\,M_\odot$ are more likely to have sSFRs comparable to SF-consistent galaxies of similar mass. This suggests that the AGNs in smaller galaxies are less effective at quenching SF as their counterparts in more massive host galaxies.

4.3. Comparison to the Literature

The masses, colors, and morphological types of these populations agree well with the literature. It has been known for decades (T. A. Matthews et al. 1964) that most radio AGNs are hosted by massive galaxies ($M_* \sim 10^{11}\,M_\odot$), a result that has been verified in the local universe (up to $z \sim 1$) with direct estimates (e.g., D. S. Heeschen 1970; R. D. Ekers & J. A. Ekers 1973; C. R. Jenkins 1982; P. N. Best et al. 2005; T. Mauch & E. M. Sadler 2007; V. Smolčić et al. 2009; M. Magliocchetti et al. 2016; J. Sabater et al. 2019; A. Capetti et al. 2022). Our sample of radio-excess AGNs also largely resides in larger galaxies, with 37% of the AGN hosts having masses $M_* > 10^{11}\,M_\odot$. Similarly, the fact that our sample of radio-excess AGNs has a redder color and resides in early-type galaxies matches canonical results. Research has established that the radio AGN host population is dominated by galaxies with older stellar populations (age ∼8–14 Gyr; e.g., L. A. Nolan et al. 2001; P. N. Best et al. 2005) and galaxies that have a lack of continuing SF (e.g., M. J. Ledlow & F. N. Owen 1995; F. Govoni et al. 2000; R. Siebenmorgen et al. 2004; D. Dicken et al. 2012). As such, radio AGNs have been shown to primarily reside in red and dead elliptical galaxies, which match the results we find in our sample. For a thorough review of the general properties of radio AGNs and their host galaxies, see the M. Magliocchetti (2022) review and references cited therein.

4.4. Mid-IR AGNs

In Section 3.2, we removed mid-IR-selected AGNs to ensure that the distribution of q was not significantly contaminated by IR emission from AGNs. We return to this sample of mid-IR AGNs to determine how many are also classified as radio-excess AGNs. Applying the $q < 1.94$ threshold, we find that of the 1103 galaxies with mid-IR-selected AGNs, 98 (∼9%) are also selected as radio-excess AGNs. This matches well with canonical evidence that has shown that ∼10%−15% of AGNs are radio-loud (e.g., K. I. Kellermann et al. 1989; D. Stern et al. 2000; see also the C. M. Urry & P. Padovani (1995) review). We note, however, that radio-loud AGNs are not exactly equivalent to radio-excess AGNs since radio-loud AGNs are typically based on absolute radio luminosities or the ratio of radio to optical fluxes, whereas radio-excess AGNs are based on the ratio of radio to IR luminosities.

The mid-IR-selected AGNs also make up a significant percentage of all the radio-selected AGNs in the full NSA-VLASS-WISE sample. Of the 723 radio-excess AGNs identified, 98 (14%) are also identified as mid-IR AGNs based on WISE color–color cuts (see Figure 9).

5. Dwarf Galaxies with Radio-excess AGNs in VLASS

5.1. Selection Criteria

Our primary goal of this work is to identify and study dwarf galaxies with radio-excess AGNs. We create a sample of dwarf galaxies from the NSA in a manner consistent with A. E. Reines et al. (2020), selecting galaxies with stellar masses $M_* \leqslant 3 \times 10^9\,M_\odot$, an upper mass limit approximately equal to the stellar mass of the Large Magellanic Cloud. Applying the mass restriction to the NSA results in a sample of 63,656 dwarf galaxies.

We cross-correlate our dwarf galaxy sample from the NSA catalog to the radio sources from VLASS, requiring a crossmatching of radius $\leqslant 2\farcs5$ (the resolution of VLASS). We find 123 matches throughout the NSA volume that meet this criterion. We crossmatch these galaxies to the AllWISE catalog with a radius of $2\farcs5$. Unlike what was done with the

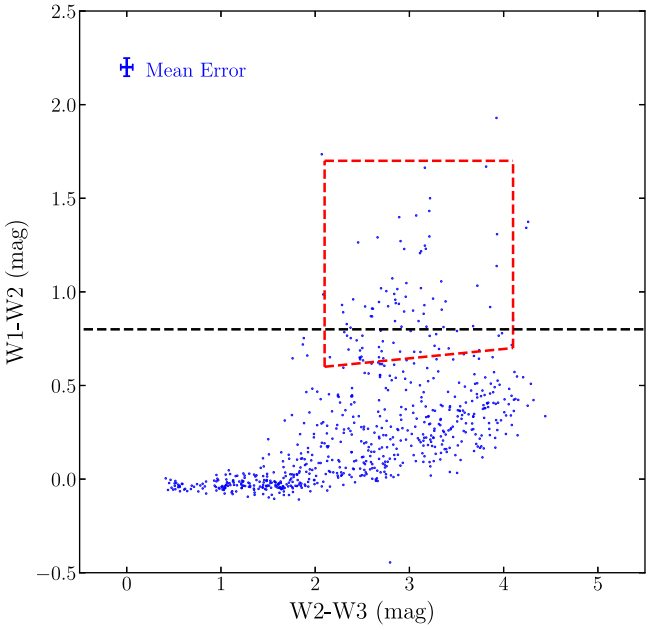

Figure 9. WISE color–color diagram for all galaxies in the NSA-VLASS-WISE sample identified as hosts for radio-excess AGNs. Approximately 14% of the radio-excess AGNs are also classified as mid-IR AGNs since they lie within the T. H. Jarrett et al. (2011) selection box (shown in red) or above the D. Stern et al. (2012) cutoff (shown in black). The mean error bars for the data are shown in the upper left corner.

full NSA-VLASS-WISE sample, we do not restrict by the WISE S/N for the dwarf galaxies for two reasons. First, we are not using the dwarf galaxies themselves to calibrate our method, and second, dwarf galaxies with VLASS detections are quite rare and we want to consider as many objects as possible. Indeed, AGN selection methods derived from more massive galaxies are often applied to dwarf galaxies for similar reasons (e.g., A. E. Reines et al. 2013; K. N. Hainline et al. 2016). We reiterate that the inclusion of galaxies with low WISE S/N does not dramatically affect the distribution of q for SFGs or the radio-excess AGN cutoff, as explained in Section 3.3. Therefore, the previously established radio-excess AGN cutoff is still valid for this sample of galaxies.

We visually inspect each of the 123 objects flagged as dwarf galaxies to eliminate interlopers. We first eliminate seven sources that are nearby H II regions. We further remove 14 objects that are distant quasars. These sources have the distinct blue, pointlike appearance of QSOs and have redshifts in SDSS that are larger than the cutoff of $z \leqslant 0.15$ employed by the NSA. We also remove one galaxy with a reported mass of 0 in the NSA, leaving 101 objects.

We inspect the spectra of the remaining galaxies to verify the redshift reported by the NSA since galaxies with unreliable redshifts will also have unreliable stellar mass estimates. We discard any galaxies whose spectra cannot be visualized in either SDSS or NED. Using the spectra from SDSS and NED, we calculate the redshifts for each of the galaxies and compare these to the redshifts reported in the NSA. If there is a discrepancy indicating the NSA redshift is erroneous, we remove the corresponding galaxy from our sample. Of the 101 galaxies, 50 have spectra in SDSS and/or NED with reliable fits that match the redshifts given by the NSA. We consider these galaxies to be bona fide dwarf galaxies.

We apply the $q < 1.94$ cutoff derived in Section 3.3 to the bona fide dwarf galaxies and find that 12 are inconsistent with SF, making them strong candidates for hosting radio-excess AGNs. Ideally, we would have enough statistical power to calibrate the selection in the mass range of interest, but this is not the case due to the small number of dwarf galaxies in VLASS. However, we note that applying the same q cutoff established from higher mass galaxies to dwarf galaxies is a very conservative method for finding AGN candidates. I. Delvecchio et al. (2021) used a sample of over 400,000 galaxies to show that the average value of q increases with decreasing stellar mass. When we divide our sample into the same stellar mass bins used by I. Delvecchio et al. (2021), we also find that the average value of q increases as stellar mass decreases. While we consider extrapolating the selection criterion down to dwarf galaxy masses, we find considerable uncertainty in the average value of q for galaxies with masses $M_* \leqslant 10^{9.5}\,M_\odot$ due to the small sample size in this mass range. Thus, we take a conservative approach and use the q cutoff derived from higher mass galaxies even though the actual cutoff value for dwarf galaxies is likely to be higher. In doing so, we may lose potential AGNs, but we create a cleaner sample of AGNs in dwarf galaxies that have excessively low q values.

We remove two of the 12 objects inconsistent with SF from our sample since they are known from other studies to *not* be AGNs associated with the dwarf host galaxies, leaving us with a final sample of 10 strong AGN candidates in dwarf galaxies. One of the two objects that we remove is the radio source in J1313+4717, which is known to host a radio-loud SNe. A. Corsi et al. (2014), N. T. Palliyaguru et al. (2019), and N. T. Palliyaguru et al. (2021) identified the radio source in J1313+4717 as a radio-loud Type Ic supernova (SN), known as PTF11qcj. PTF11qcj is a rare type of SN since most Ic SNe are **r**adio-quiet, with radio luminosities $L_\nu < 10^{19}\,\mathrm{W\,Hz^{-1}}$ (E. Berger et al. 2003; A. M. Soderberg et al. 2006; A. Corsi et al. 2016). Due to its large radio luminosity of $L_{3\,\mathrm{GHz}} \approx 6 \times 10^{21}\,\mathrm{W\,Hz^{-1}}$, it failed to be categorized as SF-consistent by the IRRC. Yet, given the extensive, multi-wavelength analysis performed on this object and its light curves, an SN is the most probable explanation for this radio source, not an AGN. The other object that we remove is the radio source in J1136+1252. This source was identified as a radio AGN in a dwarf galaxy by A. E. Reines et al. (2020; ID 64 in their paper), but follow-up spectroscopy of the bright optical point source coincident with the off-nuclear radio source has revealed it to be a background quasar at $z = 0.761$ (M. R. Sturm et al. 2024, in preparation). This source was not discarded previously because the redshift of the dwarf galaxy is correct. Only with our follow-up spectroscopy did we determine the radio source had a much higher redshift.

We provide Dark Energy Camera Legacy Survey (DECaLS) *grz*-band images of the 10 dwarf galaxies in our final sample in Figure 10 and provide VLASS images in Figure 11. For ease of reference, we assign each galaxy an ID number.

As consistency checks, we also carry out the analysis in A. E. Reines et al. (2020) and determine whether the remaining 10 radio sources can plausibly be explained by SNRs/SNe. We first use the relation between the radio luminosities of the brightest SNRs in a galaxy and the SFR of a galaxy given by L. Chomiuk & E. M. Wilcots (2009):

$$\frac{L^{\mathrm{max}}_{1.4\,\mathrm{GHz}}}{10^{24}\,\mathrm{erg\,s^{-1}\,Hz^{-1}}} = (95^{+31}_{-23}) \times \frac{\mathrm{SFR}^{0.98\pm0.12}}{M_\odot\,\mathrm{yr^{-1}}}. \quad (4)$$

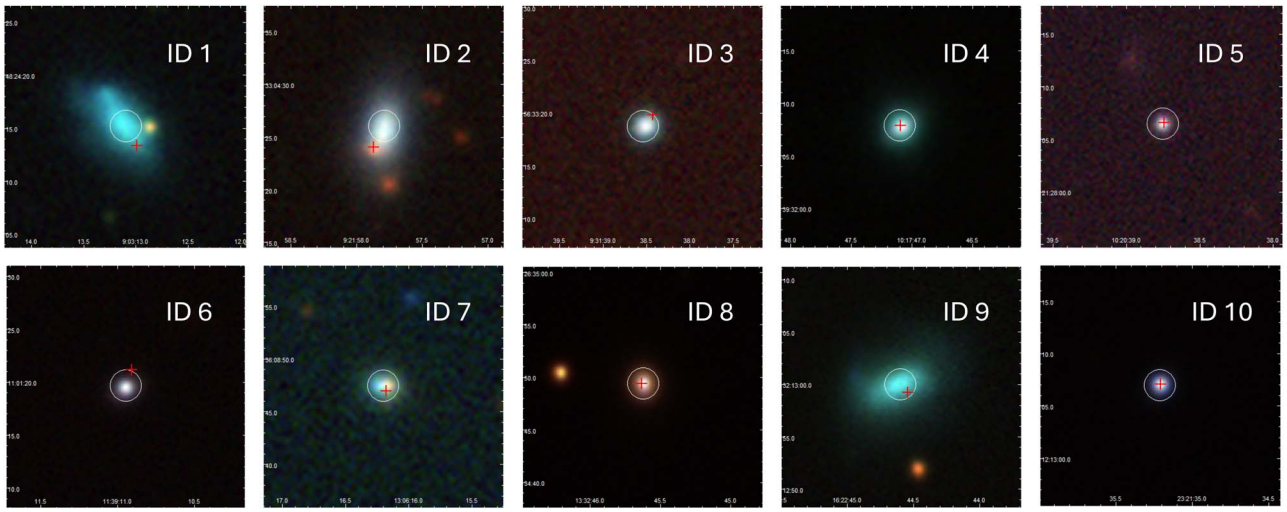

Figure 10. *grz*-band DECaLS images of the dwarf galaxies that are strong candidates for hosting radio-excess AGNs. The positions of the SDSS spectroscopic fibers with radii of 1.″5 are shown as white circles and the locations of the radio sources are shown as red crosses.

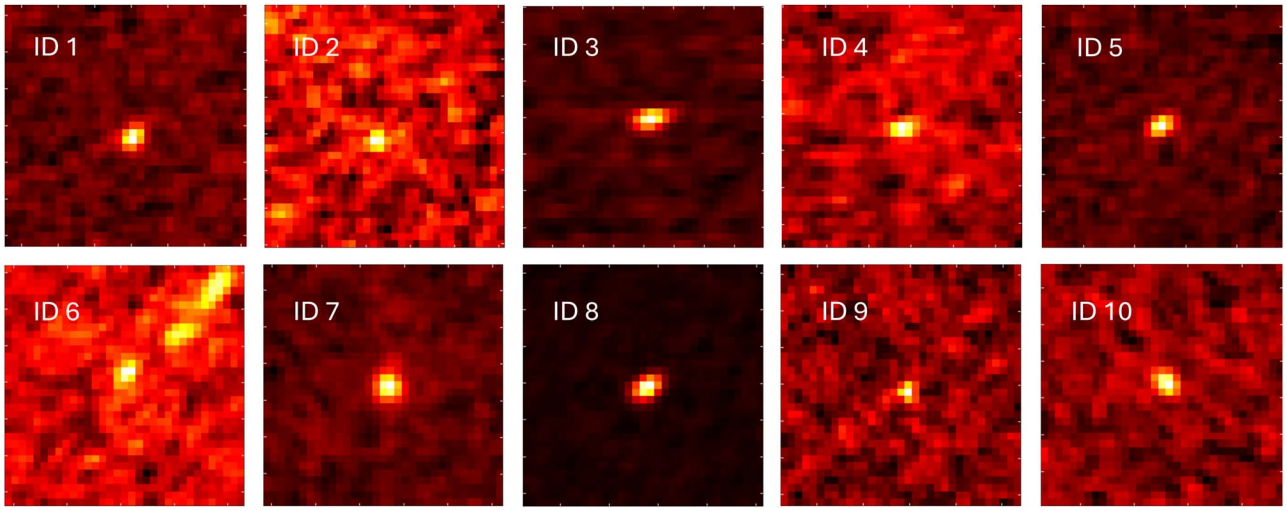

Figure 11. VLASS images of the dwarf galaxies that are strong candidates for hosting radio-excess AGNs. The images are the same angular size as the DECaLS images in Figure 10.

We convert this relation to the radio luminosities at 3 GHz using a spectral index of $\alpha = -0.5$ (L. Chomiuk & E. M. Wilcots 2009) and compare the expected luminosity from SNRs to the actual 3 GHz luminosities of the 10 radio-excess AGNs in Figure 12. We employ the SFRs calculated from Equation (3) for each galaxy. We find that the radio sources lie far above the maximum expected luminosities from individual SNRs from their galaxies, with all the sources being at least 1 mag larger than expected. As such, individual SNRs are not a likely explanation for the radio sources. For comparison, we also include Cas A, one of the youngest and most luminous SNRs in the Milky Way. Using a 1 GHz flux density of $S_{1\ \mathrm{GHz}} = 2723$ Jy and a spectral index of $\alpha = -0.770$ from J. W. M. Baars et al. (1977; epoch 1980.0), and distance of 3.4 kpc from J. E. Reed et al. (1995), we calculate a 5 GHz spectral luminosity of $L_{9\ \mathrm{GHz}} \sim 2 \times 10^{18}$ W Hz^{-1} for Cas A.

We also consider entire populations of SNRs as a possible source for compact radio emission by using the luminosity function derived in L. Chomiuk & E. M. Wilcots (2009):

$$n(L) = \frac{dN}{dL} = 92 \times \mathrm{SFR} \times L^{-2.07} \quad (5)$$

where $n(L)$ is the number of SNRs with 1.4 GHz luminosity L. We again convert from 1.4 to 3 GHz using a spectral index of $\alpha = -0.5$ (L. Chomiuk & E. M. Wilcots 2009) and calculate SFR using Equation (3).

The total expected luminosity from all SNRs in a galaxy is calculated by taking the following integral from 10^{16} to 10^{21} W Hz^{-1} to cover the range of SNRs/SNe presented in L. Chomiuk & E. M. Wilcots (2009):

$$L_{\mathrm{total}} = \int n(L)\, L\, dL. \quad (6)$$

We calculate this integral and compare the total radio luminosity from SNRs to the observed 3 GHz luminosity in Figure 13. As with the individual SNR plot, we find the actual radio luminosities to dwarf the expected radio luminosities

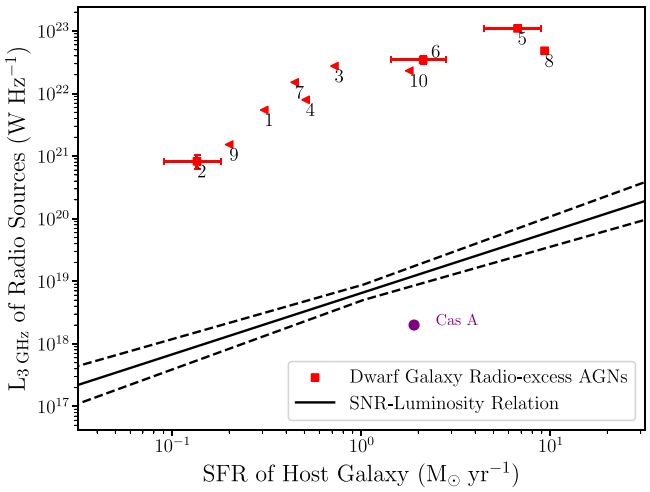

Figure 12. Radio source luminosity vs. SFR of the 10 sources identified as radio-excess AGNs in dwarf galaxies. Each source is labeled with its respective ID number (see Figure 10 and Table 1). The expected relation between SFR and radio luminosity of the brightest individual SNR/SNe from L. Chomiuk & E. M. Wilcots (2009) is shown as a solid black line, and the dashed lines show the expected scatter due to random statistical sampling. The SNR Cas A is shown for reference. The error bars for the SFR calculations are shown, and galaxies with upper limit calculations of SFR are shown as filled triangles. The 3 GHz luminosity error bars are smaller than the marker size and are not visible on the plot.

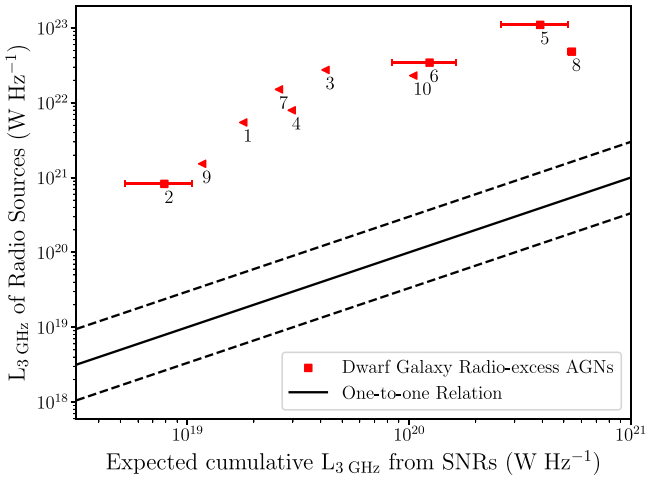

Figure 13. Observed 3 GHz luminosities vs. the predicted cumulative radio luminosities from populations of SNRs/SNe for the 10 sources identified as radio-excess AGNs in dwarf galaxies. Each source is labeled with its respective ID number. The solid black line shows the one-to-one relation, with dashed black lines offset by a factor of 3. Galaxies whose predicted cumulative luminosities are upper limits (based on Equation (6)) are shown as triangles, and the other galaxies have error bars shown. The 3 GHz luminosity error bars are smaller than the marker size and are not visible on the plot.

from the SNR population, leaving it unlikely that these phenomena are the source of the radio emission.

5.2. Potential Background Contamination

Given the small crossmatching radius of 2.″5 utilized to identify VLASS sources within dwarf galaxies, we expect the percentage of background sources to be small. We verify this hypothesis using a method like that performed in A. E. Reines et al. (2020). We estimate the number of coincidental matches found for the whole sample of dwarf galaxies from the NSA by

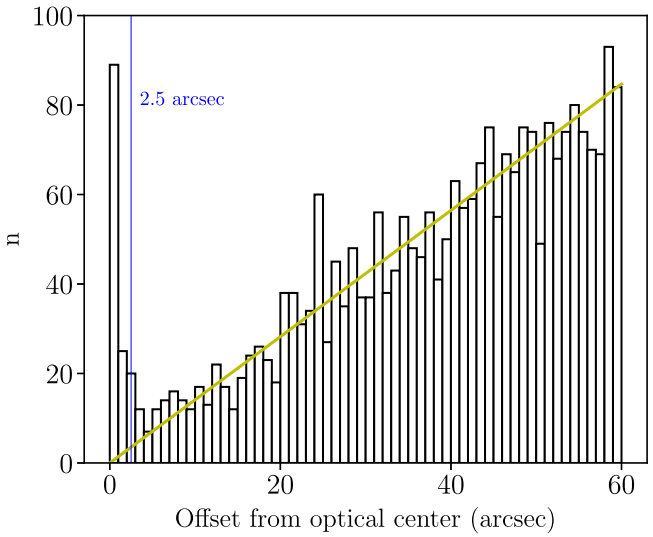

Figure 14. Observed offset distribution from crossmatching the NSA parent sample of dwarf galaxies with the VLASS radio sources, out to a matching radius of 60″. The best linear fit of the histogram is shown in yellow, and the actual crossmatching radius used to find radio sources in galaxies is shown in blue.

crossmatching the VLASS sources to the NSA galaxies out to a radius of 60″ to find the offset distribution of coincidental matches. The offset probability histogram for background sources should be a Rayleigh distribution, equal to zero at an offset of zero and rising linearly for small offsets. We fit the offset probability histogram at radii greater than 2.″5 (to ignore the bias imposed by the large number of non-coincidental matches found below 2.″5) and find the offset probability function with respect to crossmatching distance (see Figure 14). We integrate under the fit out to 2.″5 and find an expected number of $4.4 \pm \sqrt{4.4} \approx 4 \pm 2$ coincidental matches. Consequently, we expect less than 5% of the 123 radio sources to be coincidental matches between dwarf galaxies and background radio sources, meaning that statistically, less than one of the 10 dwarf galaxies with AGNs is estimated to be a background source.

5.3. General Properties

As was done with the NSA-VLASS-WISE sample, we consider several properties of the 10 radio-excess AGNs (see Table 1) to see if there are any defining characteristics of radio-excess AGNs in dwarf galaxies. We also contrast the properties of the dwarf galaxy AGNs to the AGNs in the full NSA-VLASS-WISE sample (see Section 4).

We consider the features of the radio sources in Figure 15 by plotting the 3 GHz luminosity against the size of the deconvolved major axis of each source. Following the standard employed by Y. A. Gordon et al. (2021), we find that two of the dwarf galaxy radio-excess AGNs have major axis sizes $\Psi_{maj} > 2.''5$ and are considered to be extended sources. These large major axis sizes could be explained by the AGNs having jet and core morphologies. ID 6 in particular appears to have jet-like features in its VLASS image (Figure 11). The angular size of the radio sources could also be explained by the galaxies having their synchrotron emission dominated by SF. While we utilized the IRRC to eliminate SF as the exclusive cause of the radio emission, there could be a combination of SF and AGN emission, resulting in an extended radio source. These objects

Table 1
Radio-excess AGNs in Dwarf Galaxies

ID (1)	Name (2)	NSA ID (3)	R.A. (4)	Decl. (5)	z (6)	$\log(M_*)$ (7)	$g-r$ (8)	Offset (9)	$S_{3\ \mathrm{GHz}}$ (10)	$\log(L_{3\ \mathrm{GHz}})$ (11)	Ψ_{maj} (12)	$\log(L_{1.4\ \mathrm{GHz}})$ (13)	$\log(L_{\mathrm{TIR}})$ (14)
1	J090313.09+482415.1	131284	135.8046	48.40421	0.0272	8.81	0.38	2.14	3.68(0.24)	21.74(0.03)	1.5(0.1)	21.99(0.03)	<35.90
2	J092157.79+330425.6	318231	140.4908	33.0739	0.0215	9.02	0.65	2.26	0.89(0.22)	20.92(0.11)	0(0.4)	21.15(0.11)	35.54(0.14)
3	J093138.51+563318.8	79697	142.9106	56.55521	0.0494	8.60	0.43	1.39	5.67(0.25)	22.44(0.02)	0.9(0.1)	22.67(0.02)	<36.27
4	J101747.08+393207.8	269031	154.4462	39.53552	0.0541	9.36	0.41	0.06	1.37(0.25)	21.90(0.08)	1.2(0.4)	22.13(0.08)	<36.12
5	J102038.74+212806.5	500578	155.1615	21.46847	0.1370	9.44	0.58	0.14	3.02(0.22)	23.04(0.03)	1.2(0.2)	23.29(0.03)	37.24(0.14)
6	J113910.94+110119.5	236426	174.7956	11.02212	0.0837	9.40	0.36	1.60	2.50(0.34)	22.54(0.06)	3.2(0.5)	22.77(0.06)	36.74(0.14)
7	J130616.20+360847.4	581178	196.5675	36.14651	0.0374	8.78	0.99	0.62	5.42(0.35)	22.18(0.03)	2.6(0.2)	22.40(0.03)	<36.06
8	J133245.62+263449.3	484370	203.1901	26.58038	0.0469	9.43	0.44	0.12	10.94(0.26)	22.68(0.01)	0.6(0.0)	22.96(0.01)	37.38(0.02)
9	J162244.60+321300.0	342650	245.6858	32.21666	0.0224	9.01	0.37	1.05	1.53(0.25)	21.18(0.07)	0(0.3)	21.27(0.07)	<35.71
10	J232135.20+121306.9	606795	350.3967	12.2186	0.0720	9.38	0.34	0.11	2.25(0.30)	22.36(0.06)	0(0.3)	22.60(0.06)	<36.66

Note. Column (1): galaxy ID. Column (2): galaxy name. Column (3): NSA ID (version v1_0_1). Column (4): R.A. of the galaxy from the NSA, in units of degrees. Column (5): decl. of galaxy from the NSA, in units of degrees. Column (6): redshift given by NSA. Column (7): log galaxy mass given by the NSA, in units of solar mass. Column (8): $g-r$ color given by the NSA. Column (9): offset between the Galactic center given by NSA and the radio source in VLASS, in units of arcsec. Column (10): integrated radio flux density of radio source from VLASS, in units of millijansky at 3 GHz. Column (11): log 3 GHz luminosity of radio source from VLASS, in watts per hertz. Column (12): deconvolved major axis of radio source from VLASS, in arcsec. Column (13): log 1.4 GHz luminosity of radio source from FIRST, in units of watts per hertz. Galaxies without FIRST detections have their radio luminosities estimated using a spectral index of $\alpha = -0.7$. Column (14): TIR luminosity, estimated using W4 magnitudes from WISE, in units of watts. Upper limits are indicated. The final two columns are used to calculate q. Errors for the last five columns are given in parentheses.

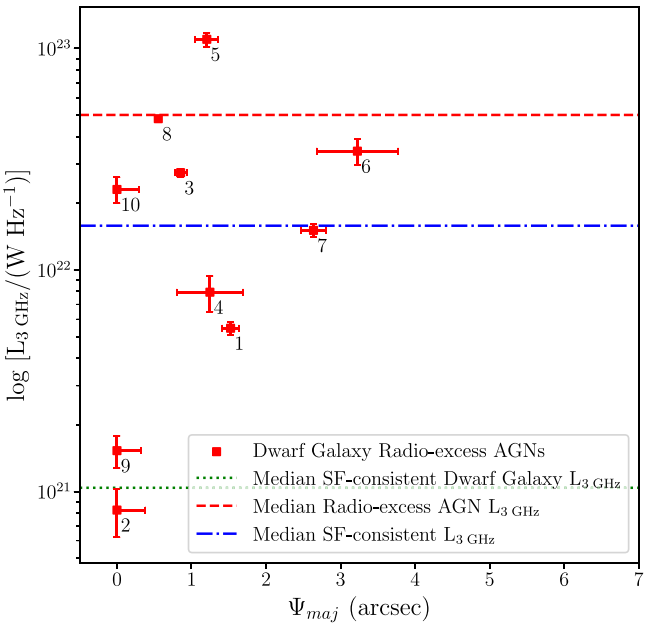

Figure 15. 3 GHz luminosities vs. deconvolved major axis sizes of the sources consistent with radio-excess AGNs in dwarf galaxies. The ID numbers for each galaxy are shown, as well as the median value of radio luminosity for the SF-consistent dwarf galaxies (green dotted line). The median values of the radio-excess AGNs and SF-consistent galaxies in the NSA-VLASS-WISE sample are also shown (red and blue lines, respectively). On average, the radio sources in the dwarf galaxies are dimmer than the radio sources of the AGNs in more massive galaxies.

would be similar to the galaxies found by H. B. Gim et al. (2019), which had low q values and signs of starburst activity, indicating the presence of both AGNs and SF. The remaining sources have smaller angular sizes and are therefore more consistent with compact sources, which is what we expect for core-dominant AGNs and is what was seen for the full NSA-VLASS-WISE sample (see Figure 5).

In contrast, the radio luminosity of the dwarf galaxy sample is inconsistent with the full AGN sample, with the radio sources in the dwarf galaxies being much dimmer than the AGNs in the full sample. Only one source (ID 5) lies above the median radio luminosity of the full radio-excess AGN population, and five of the 10 sources have 3 GHz luminosities lower than the median radio luminosity of the full SF-consistent population. Assuming the radio emission comes from AGNs, this result is not surprising since smaller galaxies are more likely to have smaller BHs that create less luminous emission. We find that the median luminosity of the SF-consistent dwarf galaxies (green dotted line in Figure 14) is much lower than the median luminosities of the full population (blue dashed–dotted line).

We consider the properties of the AGN hosts by comparing the $g-r$ colors of the galaxies to their stellar masses in Figure 16. We also compare the galaxies to the full sample of dwarf galaxies in the NSA. We find that the radio-excess AGN hosts mostly follow the trend of the entire dwarf galaxy population, making it clear that color is not a clear indicator of AGN presence in a dwarf galaxy.

We also note that only two of the dwarf galaxies with radio-excess AGNs have $g-r$ colors that are redder than the median $g-r$ color of the full SF-consistent population and only one has a redder color than the median color of the full radio-excess AGN population. This is not surprising: dwarf galaxies are bluer in general than more massive galaxies. However, this does reiterate the fact that radio-excess AGNs in dwarf galaxies do not follow the trend of more massive galaxies being found in redder galaxies.

The bluer colors of the dwarf galaxies hosting radio-excess AGNs could be explained by the fact that the AGNs in dwarf galaxies are not quenching SF as much as the AGNs in more massive galaxies. There is even the possibility that the AGNs are triggering SF in the dwarf galaxies, as was the case for the dwarf galaxy Henize 2–10 (Z. Schutte & A. E. Reines 2022).

Further differences between the full radio-excess AGN population and dwarf galaxy radio-excess population are found by analyzing the (inverse) concentration indices C (see Figure 17). Unlike the full population of radio-excess AGNs, which primarily have C values consistent with early-type galaxies (Figure 6), all of the dwarf galaxies' radio-excess AGNs have C values indicative of late-type galaxies. We note that the classification as early type and late type by the index C does not perfectly match the classification of the dwarf galaxies by eye since some of the galaxies appear irregular. While the classifications may not be accurate, the fact that the C values are larger for the dwarf galaxies shows that the dwarf galaxies are less centrally concentrated than the AGN hosts of larger mass.

We note that when A. E. Reines et al. (2020) made a similar plot of offsets versus C values for their sample of dwarf galaxy AGNs, there was a correlation between the two: higher offsets were more likely to have higher (inverse) concentration indices, seemingly indicating that more extended galaxies were more likely to host wandering AGNs. There is no clear correlation in our sample, however. If such a correlation only becomes clear at larger offsets, the maximum offset of $2\farcs5$ employed in this paper may not be large enough to make the relation discernible.

Additionally, we compare the sSFRs of the radio-excess AGNs in dwarf galaxies to the sSFRs of the full NSA-VLASS-WISE sample by plotting the SFRs against stellar masses (see Figure 18). We find that all of the radio-excess AGNs in dwarf galaxies have sSFRs higher than the median sSFR of the full AGN sample. The majority of the galaxies have sSFRs that lie above the median values of the SF-consistent population, indicating that, in general, the dwarf galaxies (including those hosting radio-excess AGNs) have larger amounts of SF than the typical galaxies in the full NSA-VLASS-WISE sample. This result matches with the $g-r$ color analysis that shows that the dwarf galaxies are bluer in color than the full sample, indicative of more recent SF. We note, of course, that several galaxies of the AGN population have upper limit detections in WISE, meaning their true location in the mass–SFR plot may be lower than what is shown.

Overall, we find that the dwarf galaxies hosting AGNs do not follow the general trends of the full population of AGN hosts. The radio sources are in general less luminous and the dwarf galaxy hosts are bluer, less centrally concentrated, and more abundant in SF than the more massive AGN hosts.

5.4. Comparison to Other AGN Detection Methods

We analyze the radio-excess AGNs in dwarf galaxies in the WISE color–color space to identify which galaxies are classified as mid-IR AGN hosts (see Figure 19). We do not restrict by WISE S/N, resulting in several galaxies with S/N < 5 in the W3 band. We plot these points with low S/N with their upper limit magnitudes in Figure 19.

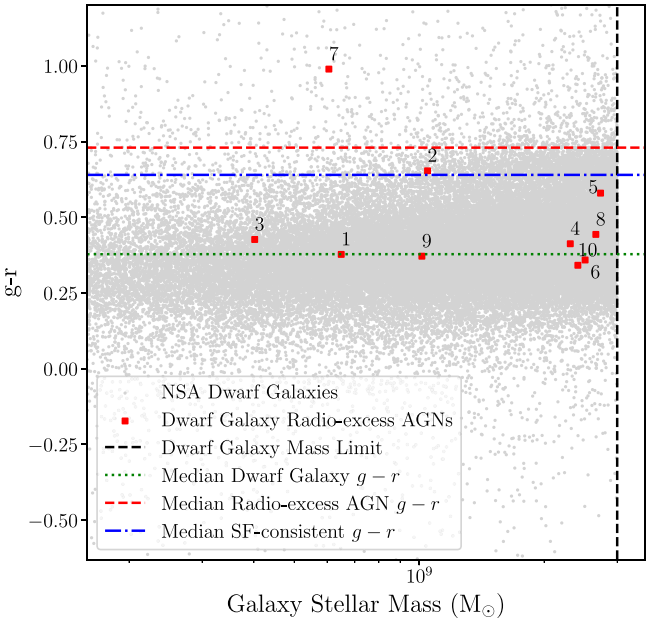

Figure 16. $g-r$ color vs. total stellar mass for dwarf galaxies ($M_* < 3 \times 10^9\ M_\odot$) in the NSA. The AGN hosts, with their associated ID numbers are shown. They mostly follow the trend of the full NSA population. The median color of all the dwarf galaxies in the NSA is shown as a green dotted line. The median colors of the radio-excess AGNs and SF-consistent galaxies in the NSA-VLASS-WISE sample are also shown, indicating that the dwarf galaxies (including the AGN hosts) are much bluer than the more massive galaxies.

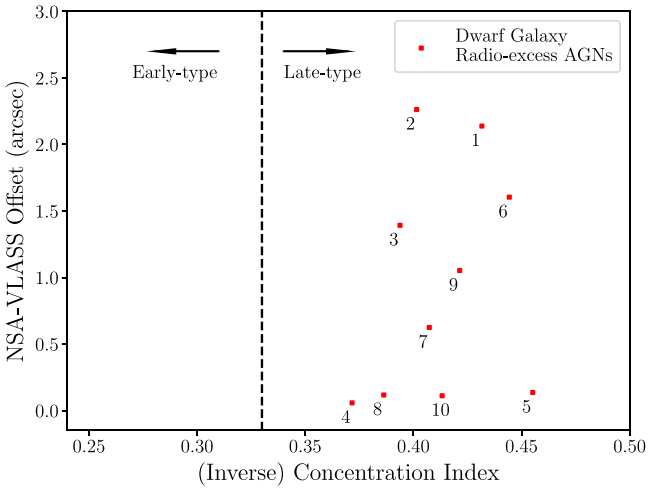

Figure 17. Offset of the radio sources in VLASS from the optical centers of their host galaxies vs. the (inverse) concentration indices, defined as $C = r_{50}/r_{90}$ (K. Shimasaku et al. 2001). Each point is labeled with the ID number of the respective galaxy. The dwarf galaxy AGN hosts have larger C values than the full population of AGN hosts (Figure 6), indicating that the dwarf galaxy hosts are less centrally concentrated than their more massive counterparts.

We find that the radio-excess AGNs in dwarf galaxies are not consistently identified as AGNs by the mid-IR selection methods: only two of the 10 AGNs are found within the T. H. Jarrett et al. (2011) box or above the D. Stern et al. (2012) cutoff. These results match well with the full population (see Figure 9), which found a similar percentage of radio-excess AGNs to be identified as AGNs with mid-IR observations.

We also analyze the 10 radio-excess AGNs in dwarf galaxies with narrow line diagnostic diagrams, using the fluxes taken from the SDSS spectral fit (Figure 20). All 10 galaxies appear

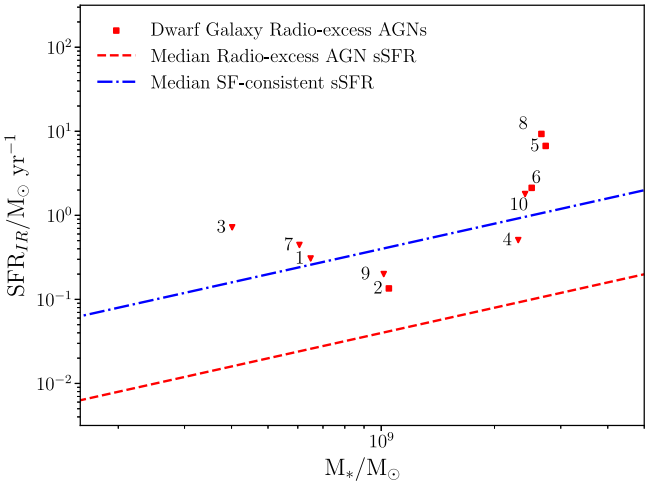

Figure 18. SFR_{IR} vs. stellar mass for the dwarf galaxies with radio-excess AGNs. SFRs calculated using upper limits in WISE are shown as triangles. The median sSFRs of the radio-excess AGN and SF-consistent populations for the full NSA-VLASS-WISE sample are also shown. In general, the dwarf galaxies have higher sSFRs than the full sample of galaxies. Each point is labeled with the ID number of the respective galaxy.

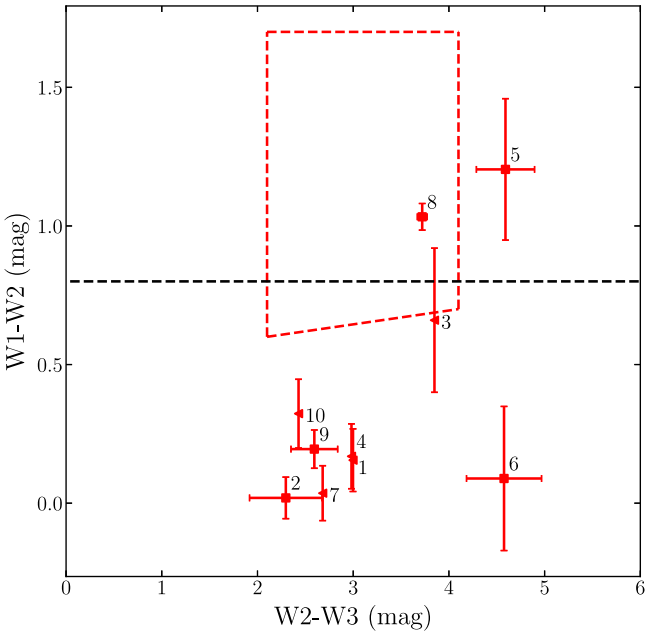

Figure 19. The WISE color–color diagram for the 10 radio-excess AGNs in dwarf galaxies. The ID number associated with each point is shown. The same AGN cutoff and selection boxes from Figures 1 and 9 are also shown. The error bars for the WISE colors are shown, and galaxies with upper limits in W3 are shown as filled red triangles. Only two of the dwarf galaxies in our AGN sample have mid-IR colors indicative of AGNs: ID 8 is found within the T. H. Jarrett et al. (2011) selection box and above the D. Stern et al. (2012) cutoff and ID 5 is only found above the D. Stern et al. (2012) cutoff. ID 3 could also be found within the T. H. Jarrett et al. (2011) selection box, due to its large uncertainty in its WISE colors.

on the [O III]/Hβ versus [N II]/Hα diagram and the [O III]/Hβ versus [S II]/Hα diagram, but only 8 appear on the [O III]/Hβ versus [O I]/Hα diagram since IDs 2 and 7 do not have reliable O I emission line fits. Most of the galaxies lie in the H II region of the emission line diagrams. These apparently contradictory results align well with the results from A. E. Reines et al.

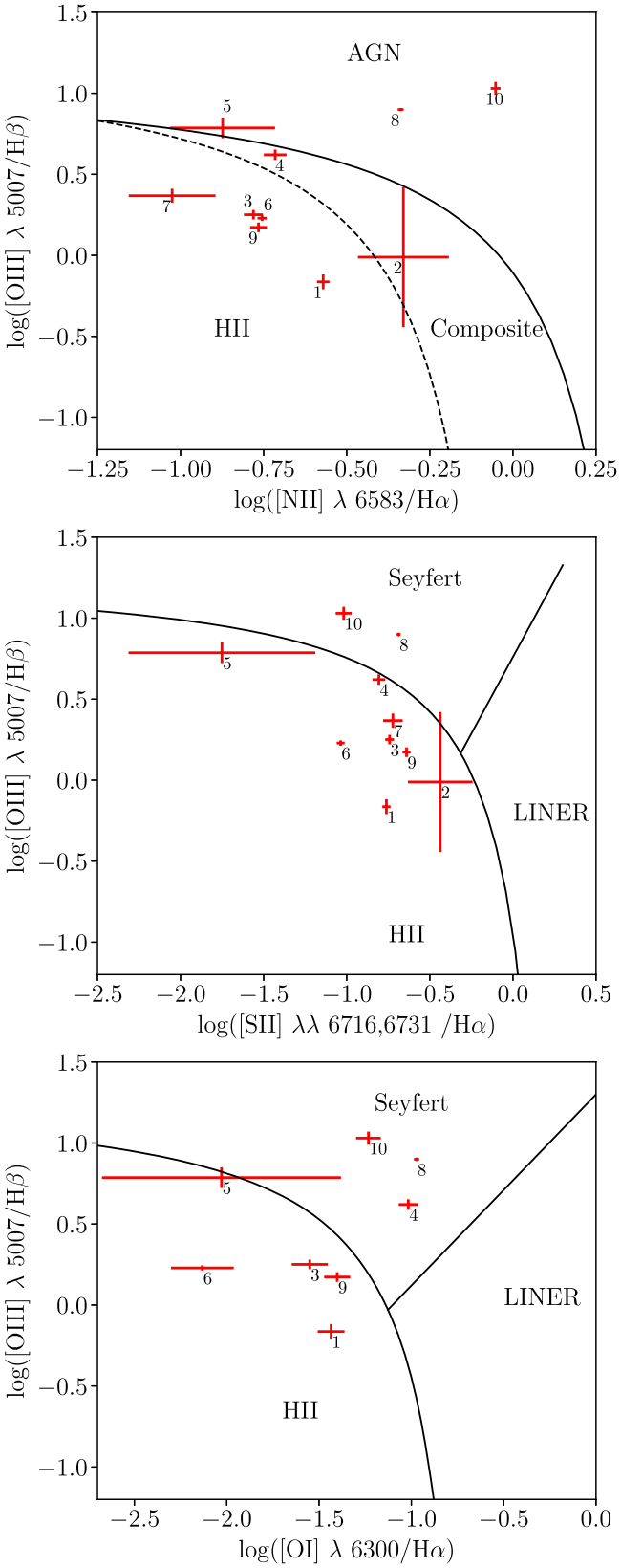

Figure 20. Optical emission line diagnostic diagrams for the dwarf galaxies with radio-excess AGNs. ID numbers for each of the galaxies in our sample are shown, along with the error bars in the measurements. The narrow line emission measurements come from the SDSS spectral fits and the divisions between regions of the diagram come from the classification scheme outlined in L. J. Kewley et al. (2006). Most of the AGN hosts lie in the SF sections of the diagrams.

(2020), which also found a majority of radio-detected AGNs in dwarf galaxies to not lie in the AGN region of the Baldwin–Phillips–Terlevich (BPT) diagrams.

Overall, the comparison between the AGN selection methods shows that the radio-excess method for finding AGNs does not correlate well with mid-IR and optical methods. Many AGNs are only identified as AGNs in the radio regime, and only two (IDs 5 and 8) are identified in AGNs in the radio, optical, and IR regimes.

5.5. Notes on Individual Galaxies

Given the small number of dwarf galaxies hosting radio-excess AGNs, we consider the properties and previous research performed on each galaxy individually, as follows:

ID 1 (J090313.1+482415.1). ID 1 has been previously identified by A. E. Reines et al. (2020) as a potential host of a wandering BH (see ID 25 in their paper). The VLASS detection is located 2.″1 away from the coordinates of its associated galaxy in SDSS and the radio source appears by eye to be distinctly offset from the center of the galaxy (see Figure 10). ID 1 was observed with the Very Large Baseline Array (VLBA) by A. J. Sargent et al. (2022), but no detections were found. However, A. J. Sargent et al. (2022) identified the radio source as an AGN by comparing the expected SFR from WISE and GALEX data to the expected SFR from FIRST data. The radio-predicted SFR was found to be excessively high, indicating that the radio emission was not likely to have come from SF alone. Therefore, this paper's classification of ID 1 as a radio-excess AGN is consistent with the classifications from A. E. Reines et al. (2020) and A. J. Sargent et al. (2022). T. Eftekhari et al. (2020) also studied ID 1 and proposed that it could be a persistent radio source associated with a fast radio burst (FRB).

ID 2 (J092157.8+330426.0). Of the 12 dwarf galaxies with radio-excess AGNs, ID 2 has the largest offset between the radio source and the optical center of its host galaxy, with an offset of 2.″3. Like ID 1, the DECaLS images (Figure 10) reveal that the radio source is not located in the nucleus of its host galaxy. The *grz*-band image from DECaLS shows a pointlike object that is prominent in the *z* band at the same location as the radio source. Given its distance from the galactic nucleus, the source is likely to be either a background AGN or a wandering BH in the dwarf galaxy. The [N II]/Hα narrow line diagnostic diagram classifies the dwarf galaxy as a composite. The radio source is undetected in FIRST, which can be explained due to the difference in sensitivities between FIRST and VLASS. VLASS reports the radio source to have a peak flux of 0.82 mJy beam^{-1}, but the catalog detection limit for FIRST in this region of the sky was 0.89 mJy beam^{-1}. The radio source was also not detected in the first epoch of VLASS, but was in the second epoch, when the depth of the survey increased.

ID 3 (J093138.5+563318.7). ID 3 was studied by A. E. Reines et al. (2020) and was identified as a radio AGN (see ID 33 in their paper). A. J. Sargent et al. (2022) also conducted a follow-up study on ID 3: while they found no VLBA detections, ID 3 was classified as an AGN based on the same SFR comparisons performed on ID 1. The classification of ID 3 in this paper is consistent with A. E. Reines et al. (2020) and A. J. Sargent et al. (2022). Although the angular offset is small (1.″4), visual inspection of the radio source finds

it to be located at the optical outskirts of its host galaxy, making it a likely candidate for a wandering BH. T. Eftekhari et al. (2020) also studied ID 3 and found its radio emission to be consistent with a persistent radio source associated with an FRB.

ID 4 (J101747.1+393207.8). VLASS found ID 4 to have a peak flux of 1.18 mJy beam^{-1}. Even though ID 4 lies in the FIRST footprint in a region of sky with a FIRST detection limit of 1.03 mJy beam^{-1}, there were no associated FIRST detections. ID 4 was also not detected in the first epoch of VLASS. The optical spectrum of ID 4 was studied in A. E. Reines et al. (2013) and was classified as a composite galaxy using BPT diagrams (ID 66 in their paper). Similarly, in the narrow line emission diagrams made with SDSS spectral fits (see Figure 20), we find ID 4 to be classified as a composite galaxy in the [N II]/Hα diagram. However, we also find it to be classified as a Seyfert in the [O I]/Hα diagram, and as a H II region by the [S II]/Hα diagram. Though the optical classifications may be unclear, the radio classification clarifies that this object is most likely a variable AGN. The morphology of ID 4 was also studied by S. J. Kimbrell et al. (2021; RGG 66) using Hubble Space Telescope observations, and was found to be an irregular galaxy with signs of undergoing a merger. Follow-up Chandra observations reveal a luminous X-ray AGN (S. J. Kimbrell & A. E. Reines 2024, in preparation).

ID 5 (J102038.7+212806.4): ID 5 is classified as an AGN by the [N II]/Hα narrow line diagnostic diagram (Figure 20) and has WISE colors consistent with an AGN (Figure 19). ID 5 was not included in A. E. Reines et al. (2020) because its redshift ($z = 0.13$) is larger than any of the redshifts included in the version of the NSA utilized by A. E. Reines et al. (2020). ID 5 was identified as a Type 2 AGN with a potential double-peaked [O II] spectrum by K. L. Smith et al. (2010). *ID 6 (J113910.9+110119.6)*: ID 6 was not included in the A. E. Reines et al. (2020) because it had a large enough redshift ($z = 0.08$) to not be included in the version of the NSA utilized by A. E. Reines et al. (2020). The radio source appears to not be centered on its host galaxy, meaning that it could be a wandering BH. The radio source is extended, and from the VLASS image, appears to have radio jets (Figure 11).

ID 7 (J130616.2+360847.4). ID 7 is the reddest of the galaxies in our sample of 13, with a $g - r$ color of 0.99. The radio source is centered on its host galaxy, making it a nuclear BH.

ID 8 (J133245.6+263449.3). A. E. Reines et al. (2013) previously identified ID 8 using optical selection methods (ID 24 in their paper). It was considered as a target for high-resolution VLA observations in A. E. Reines et al. (2020) but was cut due to scheduling priorities. ID 8 was also observed by the Chandra X-ray Observatory in L. J. Latimer et al. (2021) and its X-ray emission was higher than expected from X-ray binaries, indicating that it was likely created by an AGN (ID 5 in their paper). Furthermore, ID 8 is classified as an AGN by WISE colors (Figure 19) and by the narrow line emission diagnostics (Figure 20). Its classification as an AGN in the radio regime matches well with the classification in the IR, optical, and X-ray regimes.

ID 9 (J162244.6+321259.9). ID 9 was considered as a target for high-resolution VLA observations in A. E. Reines et al. (2020), but was cut due to scheduling priorities. ID 9 was studied by E. O. Ofek (2017), where it was shown to be consistent with a persistent radio source associated with an FRB. Although it was detected in FIRST and the second epoch of VLASS, ID 9 was not detected in the first epoch of VLASS.

ID 10 (J232135.2+121306.9). ID 10 is classified as an AGN by all three narrow line diagnostic diagrams. ID 10 has a peak VLASS flux of 2.12 mJy beam^{-1}, but did not have corresponding FIRST observations, despite being in a region in the sky with a FIRST detection limit of 0.97 mJy beam^{-1}. ID 10 also does not have any corresponding detections in the first epoch of VLASS. ID 10 is therefore a variable radio source.

5.6. Comparison to A. E. Reines et al. (2020)

Although this paper employed methods similar to those in A. E. Reines et al. (2020), the samples of radio AGNs in dwarf galaxies discovered between the two papers differ substantially. Of the 10 dwarf galaxies with radio-excess AGNs in our final sample, only two (IDs 1 and 3) were also identified as radio AGNs by A. E. Reines et al. (2020; IDs 25 and 33 in their paper). Most of the AGNs in our sample but not in A. E. Reines et al. (2020) were found due to a difference in data sets (see Section 2). Three of the galaxies here (IDs 5, 6, and 7) were not included in the older version of the NSA utilized by A. E. Reines et al. (2020). Three other galaxies (IDs 2, 4, and 10) were not detected in FIRST, which was a requirement of A. E. Reines et al. (2020); ID 2 has a VLASS flux density below the detection threshold for FIRST, and the other galaxies are likely to be variable sources that also fell below the detection limit of FIRST. The remaining two galaxies (IDs 8 and 9) were not included in A. E. Reines et al. (2020) due to VLA scheduling priorities. They both had FIRST detections, but were ultimately not followed up with high-resolution VLA observations. ID 9 notably does not have any detections in epoch 1 of VLASS, but does appear in the epoch 2 catalog.

We also investigate why many of the AGNs found in A. E. Reines et al. (2020) were not also discovered in this paper. With this paper using a more inclusive version of the NSA than A. E. Reines et al. (2020) and with VLASS having better resolution and sensitivity that covered all of the sky studied by FIRST, it is interesting to find that of the 13 radio AGNs in bona fide galaxies reported in A. E. Reines et al. (2020), only two were considered in our final dwarf galaxy sample. Here, we investigate why the other 11 were not included in our sample.

One galaxy (ID 64 in A. E. Reines et al. 2020) was discovered by our method, but was eliminated from our final sample since follow-up spectroscopy revealed it to be a background source (see Section 5.1). Another galaxy (ID 92 in A. E. Reines et al. 2020) was identified as an AGN by A. E. Reines et al. (2020) but was later identified as being consistent with SF by A. J. Sargent et al. (2022). We also found this galaxy to be consistent with SF in this paper. Four of the galaxies had optical-radio offsets above 2.″5 in A. E. Reines et al. (2020; IDs 2, 28, 48, 65 in their paper), and so were not found with our crossmatching radius of 2.″5. We choose not to increase our crossmatching radius to include these sources however, since it would increase the probability of including background sources. Indeed, A. J. Sargent et al. (2022) detected these four AGNs with VLBA observations and argued that, due to their large offset, they were statistically likely to be background sources.

The remaining galaxies not in this paper (IDs 6, 26, 77, 82, 83 in A. E. Reines et al. 2020) were not included because they did not have any corresponding detections in the VLASS

source catalog, even though they were within the VLASS footprint. Two of the sources (IDs 6 and 82) have 1.4 GHz flux densities from FIRST around 1 mJy (1.47 and 0.99 mJy, respectively), and the other sources have flux densities from FIRST above 4 mJy (A. E. Reines et al. 2020). We compare these flux densities to the detection limits of VLASS. To be listed in the VLASS catalog, a source has to have a peak flux density five times greater than the rms noise of the image. Given that VLASS has median rms noise levels of 128−145 μJy beam^{-1} (Y. A. Gordon et al. 2021), the minimum flux for a detection to be included in the VLASS catalog is in the range of 640−725 μJy beam^{-1}. The fact that the sources are not detected in VLASS indicates that the flux of the sources has changed drastically between the time of the FIRST and VLASS observations, especially for the sources with FIRST flux densities above 4 mJy. Therefore, they are likely to be variable sources. We explore the nature of the variable sources in the next section.

5.7. Variable Sources

In our individual analysis of the dwarf galaxies in our sample, we identified two galaxies (IDs 4 and 10) that were within the FIRST footprint and had large enough radio fluxes in VLASS to be detected in FIRST, but had no corresponding FIRST detections. In comparing our dwarf galaxy sample to that from A. E. Reines et al. (2020), we found the opposite: there were five galaxies (IDs 6, 26, 77, 82, and 83 from A. E. Reines et al. 2020) that had large enough fluxes in FIRST to be detected in VLASS, but had no corresponding observations in VLASS, despite being in the footprint of VLASS. We also identified one galaxy (ID 9) that had a FIRST detection and VLASS detection in epoch 2, but did not have a VLASS detection in epoch 1. We consider these sources to be radio variables and we examine possible causes of their variability.

Two possible sources of radio variability are SNe and gamma-ray bursts (GRBs). While SNe were shown to be unlikely causes of the radio emission in our sample in Section 5.1, radio-loud SNe can still create luminosities comparable to those exhibited by our variable sources. PTF11qcj, the radio-loud supernova we eliminated from our sample (Section 5.1), has a 3 GHz luminosity of $\sim10^{22}$ W Hz^{-1} in VLASS, which is a similar magnitude to the radio luminosities of the variable sources in our dwarf galaxy sample (see Table 1). The variable sources from A. E. Reines et al. (2020) also had similar radio luminosities to PTF11qcj, with 1.4 GHz luminosities of $10^{20.9}$–$10^{22.3}$ W Hz^{-1} from FIRST.

The radio luminosities of our variable sources could also be consistent with GRBs. On-axis GRBs have peak luminosities of $\sim10^{24}$ W Hz^{-1} (P. Chandra & D. A. Frail 2012), which is a magnitude larger than the luminosity of any of the variable sources in this paper or A. E. Reines et al. (2020). However, the radio emission from GRBs is variable over a timescale of around 1–2 weeks (M. Pietka et al. 2015). Since FIRST, VLASS epoch 1, and VLASS epoch 2 observations were taken years apart from each other, if a source is detected in more than one of these surveys, it is unlikely to be a GRB (e.g., ID 9 here and IDs 6 and 26[7] from A. E. Reines et al. 2020).

Tidal disruption events (TDEs; e.g., S. Komossa 2015, and references therein) are another possible source of radio variability, as stars that are ripped apart and accreted onto SMBHs create radio emission. The most luminous radio TDE, Swift J1644+57, peaked at a radio luminosity of $\sim10^{25}$ W Hz^{-1} (T. Eftekhari et al. 2018), which is larger than any of the radio luminosities of the variable sources in this paper or A. E. Reines et al. (2020). TDEs are less likely to occur with large SMBHs due to their weaker tidal fields (J. G. Hills 1975), but the smaller BHs we have discovered in dwarf galaxies could be likely candidates for TDEs. However, while TDEs are a possible source of the variability, the current literature agrees that TDEs with powerful relativistic jets are rare (e.g., S. van Velzen et al. 2018), and constitute a small percentage of the known TDE population (K. D. Alexander et al. 2020, and references therein).

While SNe, GRBs, and TDEs could be the sources of radio variability, AGNs are more likely candidates since the literature has shown that the radio variable population is dominated by AGNs (e.g., C. L. Carilli et al. 2003; K. W. Bannister et al. 2011; N. Thyagarajan et al. 2011; D. A. Frail et al. 2012; M. E. Bell et al. 2015; K. P. Mooley et al. 2016). The radio variability of AGNs can be caused by mechanisms intrinsic to the AGN or by extrinsic propagation effects, such as interstellar scattering (H. E. Bignall et al. 2015 and references therein). Follow-up observations at different radio frequencies may be performed on the variable objects noted here to create multiband spectral energy distributions that will help determine if the variability of these objects is consistent with transient phenomena, extrinsic propagation effects, or AGNs (as was done in K. Nyland et al. 2020).

6. Conclusions and Discussion

We present a large-scale search for radio-excess AGNs in dwarf galaxies using data from the second epoch of VLASS. We first develop a criterion to distinguish between SF-related radio emission and AGN radio emission by analyzing the IRRC for ∼7000 galaxies in the NSA ($z \leqslant 0.15$) across the mass scale with VLASS and WISE detections (the NSA-VLASS-WISE sample). Using our derived 2σ threshold of $q < 1.94$, we find 723 galaxies with radio-excess AGNs within this NSA-VLASS-WISE sample. We have compiled catalogs of 6904 radio-excess AGNs (including galaxies with low WISE S/N) and 6049 SF-consistent galaxies in VLASS and make these available to the community (see Appendix).

Applying the criterion to bona fide dwarf galaxies, we find 10 that are apparent hosts of radio-excess AGNs. Our statistical analysis suggests that the majority of the radio-excess AGNs in our sample are indeed associated with the dwarf host galaxies, but we cannot completely rule out partial contamination from background AGNs. Our main results on the dwarf galaxy sample are summarized below:

1. The dwarf galaxies with radio-excess AGNs starkly differ from the majority of AGN hosts in the NSA-VLASS-WISE sample. The dwarf galaxy hosts have bluer colors and larger amounts of SF than typical more massive radio-excess AGN hosts. Additionally, the dwarf galaxy hosts are not as centrally concentrated as the more massive hosts. This suggests that the dwarf hosts of radio-

[7] Note that ID 26 in A. E. Reines et al. (2020) is an optically selected AGN (ID 9 in A. E. Reines et al. 2013).

excess AGNs are similar to the general population of dwarf galaxies (e.g., Figure 16).
2. Five of the ten dwarf galaxies have evidence for hosting AGNs based on optical emission line diagnostic diagrams. Two of these also have mid-IR colors, indicating the presence of an AGN. Importantly, the emission lines confirm the AGNs are associated with the dwarf galaxies and not background sources.
3. When we compare our sample of AGNs in dwarf galaxies to the sample from A. E. Reines et al. (2020), we find evidence for eight galaxies with variable radio sources. Follow-up observations will be critical for discerning the cause of the variability of these sources.
4. Five of the dwarf galaxies with radio-excess AGNs are uniquely identified as AGNs in this paper and are prime candidates for follow-up multiwavelength observations.

The radio-excess AGNs in the dwarf galaxies presented here are probable candidates for being IMBHs. If we assume the mass of the AGNs to follow the BH mass to total stellar mass ($M_{\rm BH}$–M_*) relation from A. E. Reines & M. Volonteri (2015), we expect the BHs in these galaxies to have masses of $M \sim 10^{4.9}$–$10^{5.8}\,M_\odot$, with a median value of $10^{5.7}\,M_\odot$. We stress that there is a large amount of uncertainty in these estimates: the scatter in the A. E. Reines & M. Volonteri (2015) is quite large (0.55 dex).

This work shows the potential for finding new AGNs in dwarf galaxies using large-scale radio surveys. As such, upcoming radio facilities, such as the next-generation VLA, could be utilized to efficiently find large numbers of radio-excess AGNs in dwarf galaxies (see R. M. Plotkin & A. E. Reines 2018). Such observations will better constrain the occupation fraction of IMBHs in dwarf galaxies, which will consequently constrain the seeding models for SMBHs.

Acknowledgments

We thank the anonymous reviewer whose suggestions helped improve and clarify the manuscript. A.E.R. gratefully acknowledges support for this work provided by NSF through CAREER award 2235277 and NASA through EPSCoR grant No. 80NSSC20M0231.

Appendix

We provide the catalogs of all the radio-excess AGNs and the SF-consistent galaxies in the NSA and VLASS as machine-readable tables, and show the first five rows of each catalog in Tables A1 and A2. The AGN catalog includes galaxies that have WISE observations with low S/N. These galaxies have upper limits for their IR luminosities, but even if their IR luminosities (and the corresponding q values) are lower than the reported values, their emission is still consistent with radio-excess AGNs.

We show the spectra of the 10 dwarf galaxies that we identified as strong candidates for hosting radio-excess AGNs in Figure A1.

Table A1
Radio-excess AGNs in the NSA and VLASS

Name (1)	NSA ID (2)	R.A. (3)	Decl. (4)	z (5)	$\log(M_*)$ (6)	$g-r$ (7)	Offset (8)	$S_{3\ \mathrm{GHz}}$ (9)	$\log(L_{3\ \mathrm{GHz}})$ (10)	Ψ_{maj} (11)	$\log(L_{1.4\ \mathrm{GHz}})$ (12)	$\log(L_{\mathrm{TIR}})$ (13)
J00006.99+081645.0	613637	0.02933	8.27922	0.0394	11.34	0.81	0.28	50.90(0.41)	23.19(0.00)	0.6(0.0)	23.35(0.00)	<36.08
J000010.45+073246.9	590457	0.04357	7.54638	0.1365	11.14	0.78	0.40	5.97(0.64)	23.29(0.05)	3.7(0.4)	23.28(0.05)	<37.05
J000022.36+203412.4	605059	0.09318	20.57011	0.0734	10.84	0.80	0.55	2.01(0.45)	22.33(0.10)	4.6(1.0)	22.56(0.10)	<36.60
J000059.28-020941.3	586592	0.24700	−2.16151	0.1154	11.01	0.78	0.33	9.50(0.29)	23.44(0.01)	0(0.1)	23.99(0.01)	<37.20
J000114.33+061422.0	588788	0.30976	6.23946	0.0963	10.95	0.78	0.38	21.66(0.35)	23.56(0.01)	1.4(0.0)	23.48(0.01)	<36.78

Note. Column (1): galaxy name. Column (2): NSA ID (version v1_0_1). Column (3): R.A. of galaxy from the NSA, in units of degrees. Column (4): decl. of galaxy from the NSA, in units of degrees. Column (5): redshift given by NSA. Column (6): log galaxy mass given by the NSA, in units of solar mass, Column (7): $g-r$ color given by the NSA. Column (8): Offset between the galaxy coordinates in the NSA and the radio source location in VLASS, in units of arcsec. Column (9): integrated radio flux density of radio source from VLASS, in units of millijansky at 3 GHz. Column (10): log 3 GHz luminosity of radio source from VLASS, in units of watts per hertz. Column (11): deconvolved major axis size of radio source from VLASS, in units of arcsec. Column (12): log 1.4 GHz luminosity of radio source from FIRST, in units of watts per hertz. Galaxies without FIRST detections have their radio luminosities estimated using a spectral index of $\alpha = -0.7$. Column (13): TIR luminosity, estimated using W4 magnitudes from WISE, in units of watts. Upper limits are indicated. Errors for the last five columns are given in parentheses.

(This table is available in its entirety in machine-readable form in the online article.)

Table A2
SF-consistent Galaxies in the NSA and VLASS

Name	NSA ID	R.A.	Decl.	z	$\log(M_*)$	$g-r$	Offset	$S_{3\ \mathrm{GHz}}$	$\log(L_{3\ \mathrm{GHz}})$	Ψ_{maj}	$\log(L_{1.4\ \mathrm{GHz}})$	$\log(L_{\mathrm{TIR}})$
J000002.29-042805.0	639204	0.00993	−4.46780	0.1028	10.89	0.58	0.13	4.60(0.58)	22.96(0.06)	2.2(0.5)	23.03(0.06)	38.11(0.03)
J000009.19+252101.0	639211	0.03645	25.34987	0.0594	10.79	0.66	0.22	2.89(0.46)	22.31(0.07)	3.2(0.5)	22.54(0.07)	37.78(0.02)
J000034.96+173405.9	608760	0.14570	17.56832	0.0996	10.79	0.64	0.08	1.34(0.27)	22.42(0.09)	2.6(0.6)	22.65(0.09)	37.60(0.04)
J000040.26-054100.9	639226	0.16772	−5.68361	0.0944	10.34	0.47	0.37	2.36(0.33)	22.61(0.06)	3.6(0.7)	22.78(0.06)	38.36(0.01)
J000054.50+183021.9	639233	0.22617	18.50613	0.0563	9.68	−0.01	0.65	2.08(0.28)	22.12(0.06)	2.4(0.4)	22.35(0.06)	38.24(0.01)

Note. Same columns and units as Table A1.

(This table is available in its entirety in machine-readable form in the online article.)

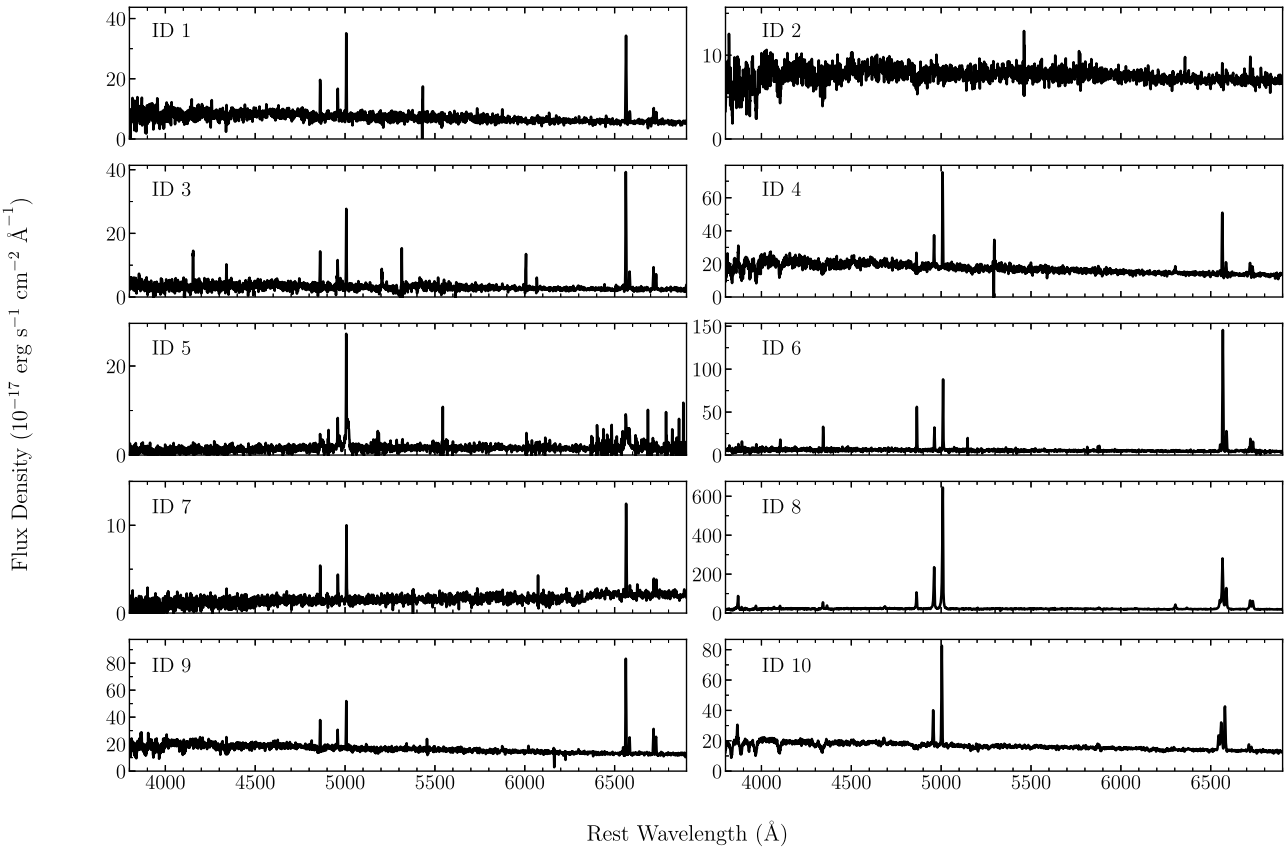

Figure A1. SDSS redshift-corrected spectra of the 10 dwarf galaxies that are strong candidates for hosting radio-excess AGNs.

ORCID iDs

Amy E. Reines https://orcid.org/0000-0001-7158-614X
Hansung B. Gim https://orcid.org/0000-0003-1436-7658
Jeremy Darling https://orcid.org/0000-0003-2511-2060
Jenny E. Greene https://orcid.org/0000-0002-5612-3427

References

Agarwal, B., Khochfar, S., Johnson, J. L., et al. 2012, MNRAS, 425, 2854
Alexander, K. D., van Velzen, S., Horesh, A., & Zauderer, B. A. 2020, SSRv, 216, 81
Baars, J. W. M., Genzel, R., Pauliny-Toth, I. I. K., & Witzel, A. 1977, A&A, 61, 99
Baldassare, V. F., Reines, A. E., Gallo, E., et al. 2016, ApJ, 829, 57
Bannister, K. W., Murphy, T., Gaensler, B. M., Hunstead, R. W., & Chatterjee, S. 2011, MNRAS, 412, 634
Bell, E. F. 2003, ApJ, 586, 794
Bell, M. E., Huynh, M. T., Hancock, P., et al. 2015, MNRAS, 450, 4221
Bentz, M. C., & Manne-Nicholas, E. 2018, ApJ, 864, 146
Berger, E., Kulkarni, S. R., Frail, D. A., & Soderberg, A. M. 2003, ApJ, 599, 408
Best, P. N., Kauffmann, G., Heckman, T. M., et al. 2005, MNRAS, 362, 25
Bignall, H. E., Croft, S., Hovatta, T., et al. 2015, in Advancing Astrophysics with the Square Kilometre Array (AASKA14) (Trieste: PoS), 58
Blanton, M. R., Eisenstein, D., Hogg, D. W., Schlegel, D. J., & Brinkmann, J. 2005, ApJ, 629, 143
Blanton, M. R., & Roweis, S. 2007, AJ, 133, 734
Bonzini, M., Padovani, P., Mainieri, V., et al. 2013, MNRAS, 436, 3759
Bruzual, G., & Charlot, S. 2003, MNRAS, 344, 1000
Capetti, A., Brienza, M., Balmaverde, B., et al. 2022, A&A, 660, A93
Caplan, J., & Deharveng, L. 1986, A&A, 155, 297
Carilli, C. L., Ivison, R. J., & Frail, D. A. 2003, ApJ, 590, 192
Chandra, P., & Frail, D. A. 2012, ApJ, 746, 156
Chomiuk, L., & Wilcots, E. M. 2009, ApJ, 703, 370
Condon, J. J. 1992, ARA&A, 30, 575
Condon, J. J., Cotton, W. D., & Broderick, J. J. 2002, AJ, 124, 675
Condon, J. J., Cotton, W. D., Fomalont, E. B., et al. 2012, ApJ, 758, 23
Condon, J. J., Kellermann, K. I., Kimball, A. E., Ivezić, Ž, & Perley, R. A. 2013, ApJ, 768, 37
Corsi, A., Gal-Yam, A., Kulkarni, S. R., et al. 2016, ApJ, 830, 42
Corsi, A., Ofek, E. O., Gal-Yam, A., et al. 2014, ApJ, 782, 42
de Jong, T., Klein, U., Wielebinski, R., & Wunderlich, E. 1985, A&A, 147, L6
Del Moro, A., Alexander, D. M., Mullaney, J. R., et al. 2013, A&A, 549, A59
Delhaize, J., Smolčić, V., Delvecchio, I., et al. 2017, A&A, 602, A4
Delvecchio, I., Daddi, E., Sargent, M. T., et al. 2021, A&A, 647, A123
Dicken, D., Tadhunter, C., Axon, D., et al. 2012, ApJ, 745, 172
Dong, X.-B., Ho, L. C., Yuan, W., et al. 2012, ApJ, 755, 167
Eftekhari, T., Berger, E., Margalit, B., Metzger, B. D., & Williams, P. K. G. 2020, ApJ, 895, 98
Eftekhari, T., Berger, E., Zauderer, B. A., Margutti, R., & Alexander, K. D. 2018, ApJ, 854, 86
Ekers, R. D., & Ekers, J. A. 1973, A&A, 24, 247
Fanaroff, B. L., & Riley, J. M. 1974, MNRAS, 167, 31P
Frail, D. A., Kulkarni, S. R., Ofek, E. O., Bower, G. C., & Nakar, E. 2012, ApJ, 747, 70
Gim, H. B., Yun, M. S., Owen, F. N., et al. 2019, ApJ, 875, 80
Gordon, Y. A., Boyce, M. M., O'Dea, C. P., et al. 2021, ApJS, 255, 30
Goulding, A. D., & Alexander, D. M. 2009, MNRAS, 398, 1165
Govoni, F., Falomo, R., Fasano, G., & Scarpa, R. 2000, A&A, 353, 507
Greene, J. E., & Ho, L. C. 2007, ApJ, 670, 92
Greene, J. E., Strader, J., & Ho, L. C. 2020, ARA&A, 58, 257
Hainline, K. N., Reines, A. E., Greene, J. E., & Stern, D. 2016, ApJ, 832, 119
Hao, C.-N., Kennicutt, R. C., Johnson, B. D., et al. 2011, ApJ, 741, 124
Heeschen, D. S. 1970, AJ, 75, 523
Helou, G., Soifer, B. T., & Rowan-Robinson, M. 1985, ApJL, 298, L7
Hills, J. G. 1975, Natur, 254, 295
Ho, L. C. 2008, ARA&A, 46, 475
Jarrett, T. H., Cohen, M., Masci, F., et al. 2011, ApJ, 735, 112
Jarrett, T. H., Masci, F., Tsai, C. W., et al. 2013, AJ, 145, 6
Jenkins, C. R. 1982, MNRAS, 200, 705
Kellermann, K. I., Sramek, R., Schmidt, M., Shaffer, D. B., & Green, R. 1989, AJ, 98, 1195

Kewley, L. J., Dopita, M. A., Sutherland, R. S., Heisler, C. A., & Trevena, J. 2001, ApJ, 556, 121
Kewley, L. J., Groves, B., Kauffmann, G., & Heckman, T. 2006, MNRAS, 372, 961
Kimball, A. E., Kellermann, K. I., Condon, J. J., Ivezić, Ž, & Perley, R. A. 2011, ApJL, 739, L29
Kimbrell, S. J., Reines, A. E., Schutte, Z., Greene, J. E., & Geha, M. 2021, ApJ, 911, 134
Komossa, S. 2015, JHEAp, 7, 148
Kormendy, J., & Ho, L. C. 2013, ARA&A, 51, 511
Kroupa, P. 2001, MNRAS, 322, 231
Lacy, M., Baum, S. A., Chandler, C. J., et al. 2020, PASP, 132, 035001
Latimer, L. J., Reines, A. E., Hainline, K. N., Greene, J. E., & Stern, D. 2021, ApJ, 914, 133
Latimer, L. J., Reines, A. E., Plotkin, R. M., Russell, T. D., & Condon, J. J. 2019, ApJ, 884, 78
Ledlow, M. J., & Owen, F. N. 1995, AJ, 109, 853
Leitherer, C., Schaerer, D., Goldader, J. D., et al. 1999, ApJS, 123, 3
Lemons, S. M., Reines, A. E., Plotkin, R. M., Gallo, E., & Greene, J. E. 2015, ApJ, 805, 12
Magliocchetti, M. 2022, A&ARv, 30, 6
Magliocchetti, M., Lutz, D., Santini, P., et al. 2016, MNRAS, 456, 431
Mateos, S., Alonso-Herrero, A., Carrera, F. J., et al. 2012, MNRAS, 426, 3271
Matthews, T. A., Morgan, W. W., & Schmidt, M. 1964, ApJ, 140, 35
Mauch, T., & Sadler, E. M. 2007, MNRAS, 375, 931
McConnell, N. J., & Ma, C.-P. 2013, ApJ, 764, 184
Mezcua, M., Civano, F., Marchesi, S., et al. 2018, MNRAS, 478, 2576
Mezcua, M., Suh, H., & Civano, F. 2019, MNRAS, 488, 685
Miller, L., Peacock, J. A., & Mead, A. R. G. 1990, MNRAS, 244, 207
Molina, M., Reines, A. E., Greene, J. E., Darling, J., & Condon, J. J. 2021, ApJ, 910, 5
Mooley, K. P., Hallinan, G., Bourke, S., et al. 2016, ApJ, 818, 105
Moran, E. C., Shahinyan, K., Sugarman, H. R., Vélez, D. O., & Eracleous, M. 2014, AJ, 148, 136
Murphy, E. J., Condon, J. J., Schinnerer, E., et al. 2011, ApJ, 737, 67
Nolan, L. A., Dunlop, J. S., Kukula, M. J., et al. 2001, MNRAS, 323, 308
Novak, M., Smolčić, V., Delhaize, J., et al. 2017, A&A, 602, A5
Nyland, K., Dong, D. Z., Patil, P., et al. 2020, ApJ, 905, 74
Ofek, E. O. 2017, ApJ, 846, 44
Palliyaguru, N. T., Corsi, A., Frail, D. A., et al. 2019, ApJ, 872, 201
Palliyaguru, N. T., Corsi, A., Pérez-Torres, M., Varenius, E., & Van Eerten, H. 2021, ApJ, 910, 16
Panessa, F., Baldi, R. D., Laor, A., et al. 2019, NatAs, 3, 387
Pietka, M., Fender, R. P., & Keane, E. F. 2015, MNRAS, 446, 3687
Plotkin, R. M., & Reines, A. E. 2018, in ASP Conf. Ser. 517, Science with a Next Generation Very Large Array, ed. E. Murphy (San Francisco, CA: ASP), 719
Reed, J. E., Hester, J. J., Fabian, A. C., & Winkler, P. F. 1995, ApJ, 440, 706
Reines, A. E. 2022, NatAs, 6, 26
Reines, A. E., & Comastri, A. 2016, PASA, 33, e054
Reines, A. E., Condon, J. J., Darling, J., & Greene, J. E. 2020, ApJ, 888, 36
Reines, A. E., Greene, J. E., & Geha, M. 2013, ApJ, 775, 116
Reines, A. E., & Volonteri, M. 2015, ApJ, 813, 82
Ricarte, A., & Natarajan, P. 2018, MNRAS, 481, 3278
Rose, S. C., Naoz, S., Sari, R., & Linial, I. 2022, ApJL, 929, L22
Sabater, J., Best, P. N., Hardcastle, M. J., et al. 2019, A&A, 622, A17
Salehirad, S., Reines, A. E., & Molina, M. 2022, ApJ, 937, 7
Sargent, A. J., Johnson, M. C., Reines, A. E., et al. 2022, ApJ, 933, 160
Satyapal, S., Abel, N. P., & Secrest, N. J. 2018, ApJ, 858, 38
Schutte, Z., & Reines, A. E. 2022, Natur, 601, 329
Schutte, Z., Reines, A. E., & Greene, J. E. 2019, ApJ, 887, 245
Shimasaku, K., Fukugita, M., Doi, M., et al. 2001, AJ, 122, 1238
Siebenmorgen, R., Freudling, W., Krügel, E., & Haas, M. 2004, A&A, 421, 129
Smith, K. L., Shields, G. A., Bonning, E. W., et al. 2010, ApJ, 716, 866
Smolčić, V., Novak, M., Bondi, M., et al. 2017, A&A, 602, A1
Smolčić, V., Zamorani, G., Schinnerer, E., et al. 2009, ApJ, 696, 24
Soderberg, A. M., Nakar, E., Berger, E., & Kulkarni, S. R. 2006, ApJ, 638, 930
Stern, D., Assef, R. J., Benford, D. J., et al. 2012, ApJ, 753, 30
Stern, D., Djorgovski, S. G., Perley, R. A., de Carvalho, R. R., & Wall, J. V. 2000, AJ, 119, 1526
Thyagarajan, N., Helfand, D. J., White, R. L., & Becker, R. H. 2011, ApJ, 742, 49
Truebenbach, A. E., & Darling, J. 2017, MNRAS, 468, 196
Urry, C. M., & Padovani, P. 1995, PASP, 107, 803
van Velzen, S., Bower, G. C., & Metzger, B. D. 2018, in ASP Conf. Ser. 517, Science with a Next Generation Very Large Array, ed. E. Murphy (San Francisco, CA: ASP), 737
Volonteri, M., Lodato, G., & Natarajan, P. 2008, MNRAS, 383, 1079
Volonteri, M., & Natarajan, P. 2009, MNRAS, 400, 1911
White, R. L., Becker, R. H., Helfand, D. J., & Gregg, M. D. 1997, ApJ, 475, 479
Wright, E. L., Eisenhardt, P. R. M., Mainzer, A. K., et al. 2010, AJ, 140, 1868
Wright, E. L., Eisenhardt, P. R. M., Mainzer, A. K., et al. 2019, AllWISE Source Catalog, IPAC, doi:10.26131/IRSA1
York, D. G., Adelman, J., & Anderson, J. E. 2000, AJ, 120, 1579
Yun, M. S., Reddy, N. A., & Condon, J. J. 2001, ApJ, 554, 803
Zakamska, N. L., Lampayan, K., Petric, A., et al. 2016, MNRAS, 455, 4191